Generation of number-phase minimum-uncertainty states and number states

Y. Yamamoto, S. Machida, N. Imoto, M. Kitagawa, and G. Björk*

NTT Electrical Communication Laboratories, 3-9-11, Midoricho, Musashinoshi, Tokyo 180, Japan

Received February 5, 1987; accepted July 6, 1987

The difference between the two nonclassical photon states, i.e., the squeezed state and the number-phase minimum-uncertainty state, is discussed. Four different generation principles for number-phase minimum-uncertainty states (and number states) are described. They are the following: (1) unitary evolution, using self-phase modulation and interference; (2) nonunitary state reduction, using either quantum nondemolition photon-number measurement or parametrically amplified idler-wave photon counting; (3) negative-feedback oscillators, incorporating a correlated photon-pair generator; and (4) pump-amplitude noise-suppressed lasers. A number-phase minimum-uncertainty state with photon-number noise reduced to 1 dB (20%) below the standard quantum limit in a frequency range over 100 MHz was produced by the fourth-generation principle.

1. INTRODUCTION

The Heisenberg uncertainty principle for two conjugate observables $\hat{O}_1$ and $\hat{O}_2$ is the direct consequence of the commutation relation between them. It can be derived by the Schwartz inequality[1]

$$[\hat{O}_1, \hat{O}_2] = i\hat{O}_3 \rightarrow \langle \Delta\hat{O}_1{}^2\rangle\langle \Delta\hat{O}_2{}^2\rangle \geqq \frac{1}{4}|\langle \hat{O}_1, \hat{O}_2\rangle|^2 = \frac{1}{4}\langle \hat{O}_3\rangle^2, \tag{1.1}$$

where $\Delta\hat{O}_i = \hat{O}_i - \langle \hat{O}_i\rangle, i = 1, 2$. A state that exactly satisfies the equality in Eq. (1.1) is called a minimum-uncertainty state and is mathematically defined as an eigenstate of the operator[2]

$$\hat{O}(r) = e^r\hat{O}_1 + ie^{-r}\hat{O}_2, \tag{1.2}$$

where r is a squeezing parameter. That is, r determines the distribution of quantum noise between $\hat{O}_1$ and $\hat{O}_2$:

$$\left.\begin{aligned}\langle \Delta\hat{O}_1{}^2\rangle &= \langle \Delta\hat{O}_1{}^2\rangle_{r=0}e^{-2r}\\ \langle \Delta\hat{O}_2{}^2\rangle &= \langle \Delta\hat{O}_2{}^2\rangle_{r=0}e^{2r}\end{aligned}\right\} \text{(minimum-uncertainty product).} \tag{1.3}$$

A squeezed state (SS) of the electromagnetic field[3–6] is one of minimum-uncertainty states, in which $\hat{O}_1$ and $\hat{O}_2$ correspond to the two quadrature phase components $\hat{a}_1 = \frac{1}{2}(\hat{a} + \hat{a}^\dagger)$ and $\hat{a}_2 = (1/2i)(\hat{a} - \hat{a}^\dagger)$. $\hat{O}_3$ is then a c number (=1/2). The SS features reduced quantum noise in one quadrature and enhanced quantum noise in the other quadrature. In the special case of $r = 0$, the two quadrature components share the same amount of quantum noise, namely, $\langle \Delta\hat{a}_1{}^2\rangle = \langle \Delta\hat{a}_2{}^2\rangle = 1/4$. This is Glauber's coherent state[7] (CS). The electromagnetic field generated by a classical current is in a CS.[8] Its quadrature-component quantum noise is sometimes referred to as the standard quantum limit (SQL). In order to ultimately reduce the noise in one of the quadratures to zero in a SS (such a state is called a quadrature-phase state), the electromagnetic-field mode must have an infinite photon number and thus an infinite energy. This is because the enhanced quadrature noise component will require part of the total photon number[5]

$$\langle \hat{n}\rangle_{SS} = \langle \hat{a}_1\rangle^2 + \langle \hat{a}_2\rangle^2 + \sinh^2(r) \xrightarrow[(r\rightarrow\infty)]{} \infty. \tag{1.4}$$

That is, there is a trade-off relation between quantum-noise reduction and the required photon number in a SS.

A number-phase minimum-uncertainty state (NUS) of the electromagnetic field is defined as

$$\hat{O}_1 = \hat{n} \equiv \hat{a}^\dagger\hat{a}, \quad \hat{O}_2 = \hat{S} \equiv \frac{1}{2i}[(\hat{n}+1)^{-1/2}\hat{a} - \hat{a}^\dagger(\hat{n}+1)^{-1/2}] \tag{1.5}$$

and

$$\hat{O}_3 = \hat{C} \equiv \tfrac{1}{2}[(\hat{n}+1)^{-1/2}\hat{a} + \hat{a}^\dagger(\hat{n}+1)^{-1/2}], \tag{1.6}$$

where $\hat{n}$, $\hat{S}$, and $\hat{C}$ are the photon-number operator, the sine operator, and the cosine operator,[9] respectively. When r is equal to $-\frac{1}{2}\ln(2\langle\hat{n}\rangle)$ and the average photon number is much greater than unity, the photon-number noise and the sine-operator noise (which corresponds to the classical phase noise) are reduced to $\langle(\Delta\hat{n})^2\rangle = \langle\hat{n}\rangle$ and $\langle(\Delta\hat{S})^2\rangle = [(\langle\hat{C}\rangle^2)/(4\langle n\rangle)] \cong 1/(4\langle\hat{n}\rangle)$. A CS is not a NUS, yet it approximately satisfies the above photon-number and sine-operator noise when its photon number is much greater than unity.[10] Therefore this number and sine-operator noise is also referred to as the SQL. A NUS with r greater than $-\frac{1}{2}\ln(2\langle\hat{n}\rangle)$ features smaller photon-number noise and larger sine-operator noise than the SQL, while the minimum-uncertainty relationship $\langle(\Delta\hat{n})^2\rangle\langle(\Delta\hat{S})^2\rangle = \frac{1}{4}\langle\hat{C}\rangle^2$ is preserved. The photon-number noise can ultimately be reduced to zero (photon-number state) without requiring an infinite photon number, because the enhanced phase noise does not require any photons at all.

The quantum-statistical properties of these photon states are conveniently described by the density operator $\hat{\rho} = |\psi\rangle\langle\psi|$, where $|\psi\rangle$ is the state's wave function.

The difference between the above photon states is described by the quasi-probability density (Q representation)

0740-3224/87/101645-18$02.00

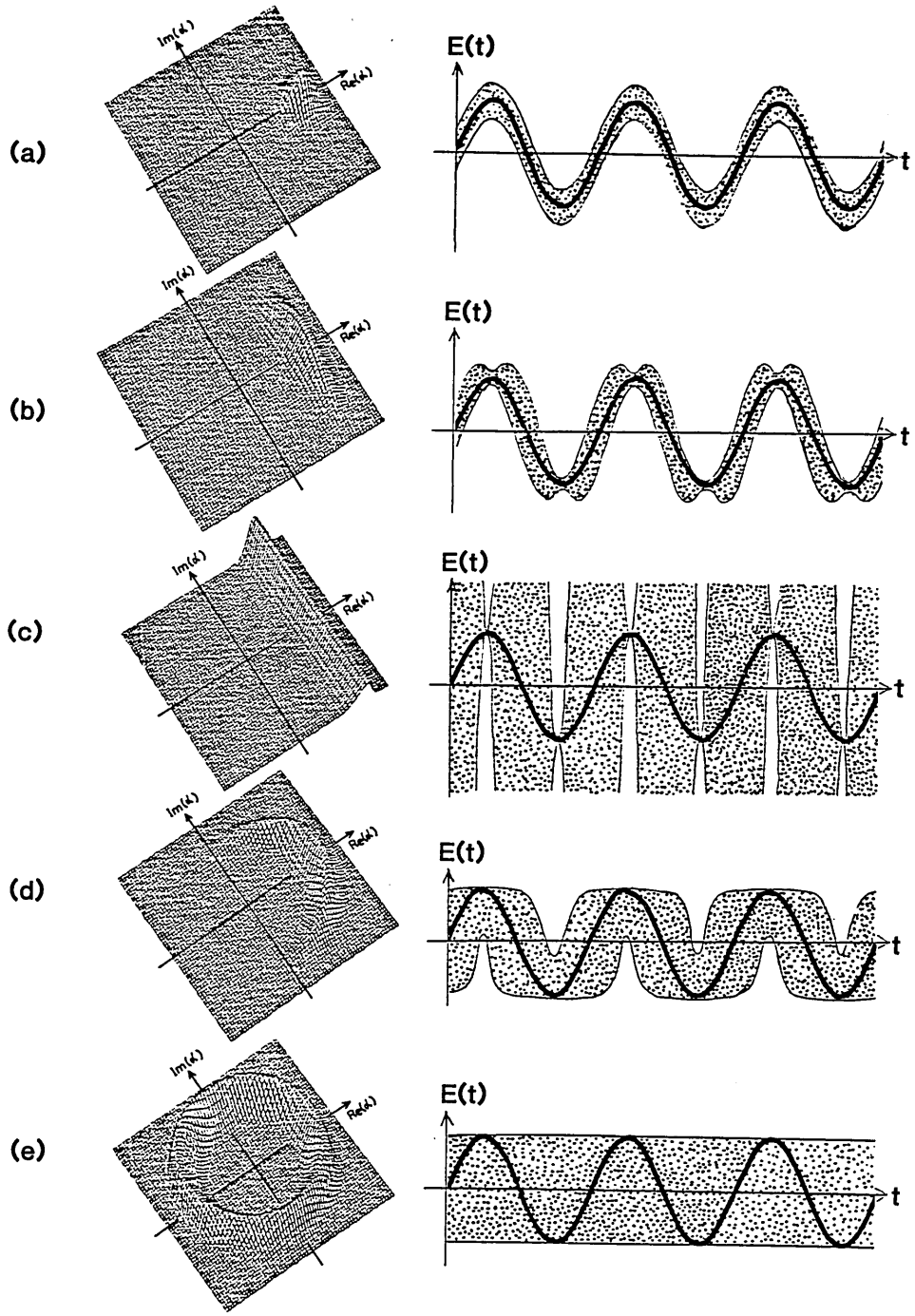

Fig. 1. Quasi-probability densities $Q(\alpha)$ and electric fields $E(t)$. (a) CS, (b) SS, (c) quadrature-phase eigenstate of $\hat{a}_1$, (d) NUS, and (e) number state.

$$Q(\alpha) \equiv \langle \alpha | \hat{\rho} | \alpha \rangle = |\langle \alpha | \psi \rangle|^2, \tag{1.7}$$

where $|\alpha\rangle$ is a CS with the complex eigenvalue α and the real and imaginary parts of α corresponds to $\langle \hat{a}_1 \rangle$ and $\langle \hat{a}_2 \rangle$, respectively. Neither a SS or a NUS possesses a positive-definite diagonal $P(\alpha)$ function for the density operator, which implies that these states cannot be realized by a classical mixture of CS. The term "nonclassical photon states" has been coined because of this fact.

Figure 1 compares the quasi-probability densities $Q(\alpha)$ and the intuitive electromagnetic fields of a CS, a SS, a quadrature-phase state, a NUS, and a number state.

Generation of a NUS as well as a SS is of potential importance for communication, information processing, precision measurement, and atomic spectroscopy. A photon-number state, specifically, achieves the maximum channel capacity in optical communication[11] and also realizes a photonic-reversible computer.[12] It also improves the performance of gravity-wave-detecting interferometers.[13]

An unmistakable mark of SS generation is the observation of quadrature phase squeezing. That is, a homodyne-detector output current will feature a reduced noise level below that for vacuum fields.[14–17] An unmistakable mark of NUS generation, on the other hand, is the observation of ampli-

tude squeezing. That is, a photon-counting detector output will feature a noise level below the shot-noise level and thus sub-Poissonian photon statistics. As can be seen from Fig. 1, though, these characteristics are also featured by SS when the squeezing parameter is relatively small.

In this paper we discuss four different generation principles for NUS and report on the first observation to our knowledge of amplitude squeezing. A unitary operator and its physical realization for transforming a CS to a NUS are presented in Section 2.[18] The similarity and difference between the unitary operators for SS generation and NUS generation are discussed. The nonunitary state reduction by quantum measurement is discussed in Section 3 as an alternative way to generate a NUS.[19] The quantum-nondemolition (QND) photon-number measurement using the optical Kerr effect[20] and parametrically amplified idler photon counting[21] are demonstrated as such examples. In Section 4 we discuss the measurement–feedback combination, which continuously produces a NUS with a prescribed eigenvalue and eigenfunction. The QND feedback laser oscillator[22] and the idler feedback parametric oscillator[23,24] are discussed as such schemes. Finally, in Section 5 we treat a dissipative (open) system, which establishes macroscopic quantum coherence through the balance between the system's ordering force and the reservoirs' fluctuating forces. Favorable control of the balance leads to a NUS generation instead of a CS generation. A saturated laser oscillator with suppressed pump-amplitude fluctuation[25,26] is discussed as an example. The observation of amplitude squeezing in a pump-noise-suppressed semiconductor laser is briefly described.[27] The four different generation principles are shown schematically in Fig. 2.

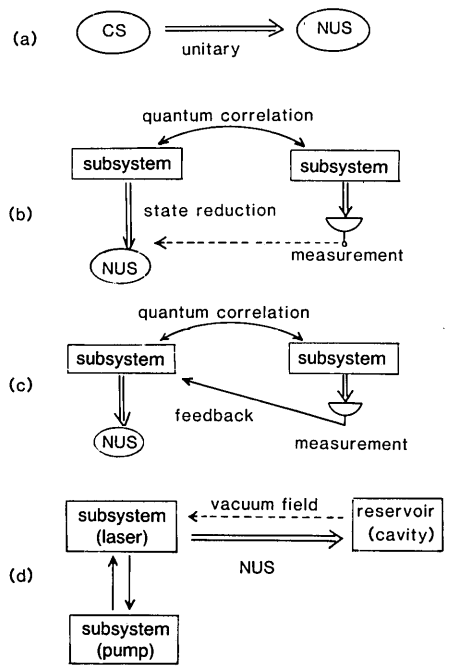

Fig. 2. Four generation principles for NUS's: (a) unitary transformation, (b) nonunitary state reduction by measurement, (c) measurement-feedback combination, (d) pump-noise-suppressed laser oscillator.

2. UNITARY EVOLUTION FOR NUMBER-PHASE MINIMUM-UNCERTAINTY STATE GENERATION

In this section we compare the two unitary evolutions that generate a SS and a NUS, respectively, from a CS.

A. Two-Photon Interaction for Squeezed-State Generation

The interaction Hamiltonian for the unitary evolution generating SS is quadratic in photon-annihilation and -creation operators[5,6]:

$$H_I = \frac{\hbar}{2}(\chi \hat{a}^{\dagger 2} + \chi^* \hat{a}^2). \tag{2.1}$$

This implies simultaneous two-photon generation and absorption that are due to the second- or third-order nonlinearities:

$$\chi = \begin{cases} \chi^{(2)}\epsilon, & \text{parametric amplification} \\ \chi^{(3)}\epsilon^2, & \text{four-photon mixing} \end{cases}, \tag{2.2}$$

where ϵ is the (classical) pump field.

The state evolution in the Schrödinger picture resulting from this *two-photon interaction* is expressed as

$$|\psi\rangle_{\text{out}} = U_2(L)|\psi\rangle_{\text{in}}, \tag{2.3}$$

where the unitary operator $U_2(L)$ is given by

$$U_2(L) = \exp\left[\frac{iL}{2v}(\chi^* \hat{a}^2 + \chi \hat{a}^{\dagger 2}\right], \tag{2.4}$$

where v is the velocity of light in the nonlinear medium and L is the interaction length. The output mode operator $\hat{a}_{\text{out}}$ in the Heisenberg picture is, on the other hand, written in terms of the input operator $\hat{a}_{\text{in}}$:

$$\hat{a}_{\text{out}} \equiv U_2^\dagger \hat{a}_{\text{in}} U_2 = \hat{a}_{\text{in}} \cosh(r) - \hat{a}_{\text{in}}^\dagger e^{i\theta} \sinh(r), \tag{2.5}$$

where $re^{i\theta} = -i\chi L/v$ (r is a real c number) and θ depends on the phase of the pump wave. When $\theta = 0$, the two quadrature components of the output mode are squeezed as follows:

$$\langle(\Delta\hat{a}_{\text{out},1})^2\rangle = \langle(\Delta\hat{a}_{\text{in},1})^2\rangle e^{-2r}$$

and

$$\langle(\Delta\hat{a}_{\text{out},2})^2\rangle = \langle(\Delta\hat{a}_{\text{in},2})^2\rangle e^{2r}. \tag{2.6}$$

When the input state is in a CS, $|\psi\rangle_{\text{in}} = |\alpha_{\text{in}}\rangle$, the output state is in a SS with the squeezing parameter r.

The density operator of the output state is written as

$$\rho_{\text{out}} \equiv |\psi\rangle_{\text{out out}}\langle\psi| = U_2|\alpha_{\text{in}}\rangle\langle\alpha_{\text{in}}|U_2^\dagger. \tag{2.7}$$

The quasi-probability density (Q representation) of Eq. (2.7) is compared with that for a CS in Fig. 1. The circular noise distribution of a CS is deformed to an elliptical noise distribution because of the unitary operation U_2. Note that this is either an amplification or a deamplification process for the coherent excitation of the signal.

The quadratic Hamiltonian [Eq. (2.1)] is realized by a degenerate parametric amplifier, as originally proposed by Takahashi.[3] It is also realized by a degenerate four-photon mixer as proposed by Yuen and Shapiro.[28] In this scheme, the modes are degenerate (or nearly degenerate) in frequency, yet they belong to different spatial modes. The recent

experimental observations of SS[14,16] utilized slightly modified versions (use of a cavity) of these two basic schemes. If the signal and pump modes are in the same spatial mode and are different only in frequency,[15,17] the output state resembles a NUS more than a SS, which will be discussed next.

B. Four-Photon Interaction for Number-Phase Minimum-Uncertainty State Generation

The interaction Hamiltonian for the unitary evolution generating a NUS is quartic in photon-annihilation and -creation operators[18]:

$$H_I = \hbar\chi\hat{a}^{\dagger 2}\hat{a}^2. \tag{2.8}$$

No photon absorption or emission is involved, so that the signal photon number is preserved.

The state evolution in the Schrödinger picture that results from this *four-photon interaction* is expressed by the new unitary operator

$$U_4(L) = \exp\left[i\chi\frac{L}{v}(\hat{a}^{\dagger 2}\hat{a}^2)\right] = \exp\left[i\frac{\gamma}{2}\hat{n}(\hat{n}-1)\right], \tag{2.9}$$

where $\gamma = 2\chi L/v$ is the nonlinear interaction parameter. The output mode operator $\hat{a}'_{\text{out}}$ in the Heisenberg picture can then be written in terms of $\hat{a}_{\text{in}}$:

$$\hat{a}'_{\text{out}} \equiv U_4^{\dagger}\hat{a}_{\text{in}}U_4 = e^{i\gamma\hat{n}}\hat{a}_{\text{in}}. \tag{2.10}$$

This is the so-called self-phase-modulation process. The phase of the output mode is quantum-mechanically correlated with its photon number as indicated by Eq. (2.10), yet the photon-number statistics still remain Poissonian if the input is a CS. The Q representation for the self-phase modulated CS is depicted in Fig. 3(a). Since a quantum-mechanical correlation is established between the photon number and phase by the unitary evolution [Eq. (2.9)], it is anticipated that the photon-number noise can be reduced below the SQL, for instance, by an interference process. An interference effect at a low-reflectivity mirror can be expressed by the unitary displacement operator

$$D(\xi) = \exp(\xi\hat{a}^{\dagger} - \xi^*\hat{a}), \tag{2.11}$$

and

$$\hat{a}_{\text{out}} \equiv D^{\dagger}\hat{a}'_{\text{out}}D = \hat{a}'_{\text{out}} + \xi, \tag{2.12}$$

where ξ is a complex c number that represents the classical coherent excitation added to the signal wave through the mirror. The overall unitary operator for NUS generation is given by

$$U_T \equiv D(\xi)U_4(L) = \exp(\xi\hat{a}^{\dagger} - \xi^*\hat{a})\exp\left[i\frac{\gamma}{2}\hat{n}(\hat{n}-1)\right]. \tag{2.13}$$

The output mode operator in the Heisenberg picture after the overall interaction is written as

$$\hat{a}_{\text{out}} \equiv U_T^{\dagger}\hat{a}_{\text{in}}U_T = e^{i\gamma\hat{n}}\hat{a}_{\text{in}} + \xi. \tag{2.14}$$

The excitation ξ added through the low-reflectivity mirror must be optimized to minimize the photon-number noise of the output mode $\hat{a}_{\text{out}}$, as shown in Fig. 3(a). For this purpose, ξ must be $-\pi/2$ out of phase from the coherent excitation of $\hat{a}_{\text{out}}$. Figure 3(b) shows the normalized photon-number noise (Fano factor) $\langle(\Delta\hat{n}_{\text{out}})^2\rangle/\langle\hat{n}_{\text{out}}\rangle$ versus the nonlinear interaction parameter γ, where the photon-number noise has been minimized by the optimum ξ value. When γ is increased, the photon-number noise is first decreased to below the SQL but is increased again beyond a certain γ value. This optimum γ value is

$$\gamma_1 = \frac{1}{2}\langle\hat{n}_{\text{out}}\rangle^{-2/3}. \tag{2.15}$$

The minimum photon-number noise that is realized at $\gamma = \gamma_1$ is

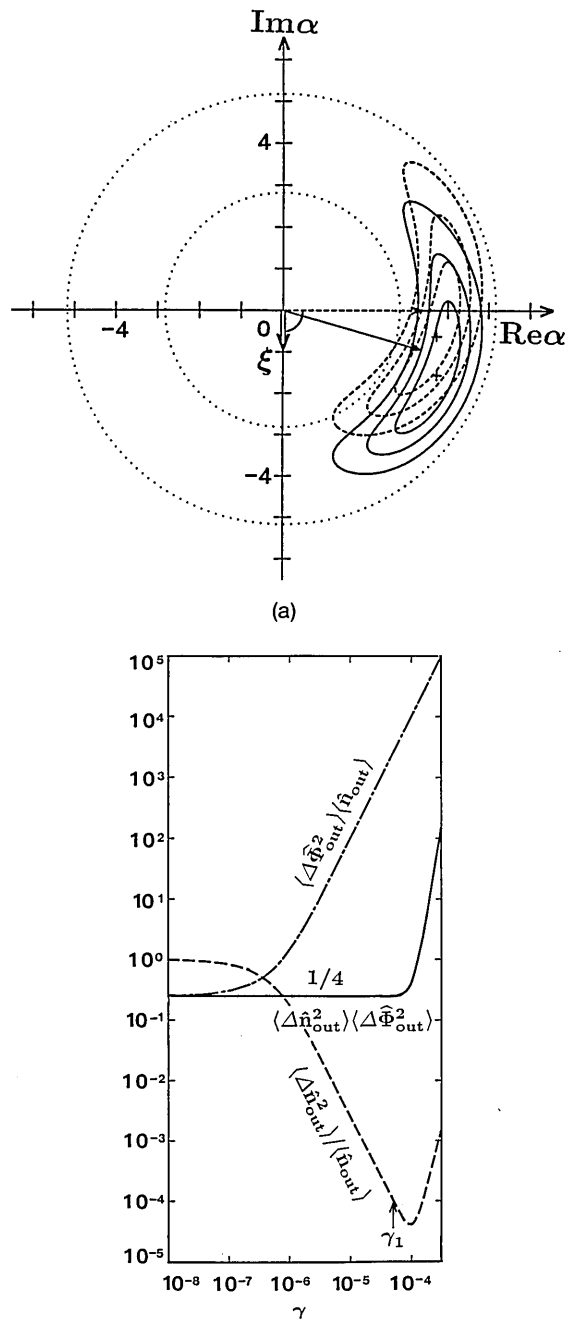

Fig. 3. (a) Changes of $Q(\alpha)$ by self-phase modulation in the Kerr medium and by the interference at the output mirror. $Q(\alpha)$ indicated by dashed contours is shifted to solid contours by the interference. Contours are drawn for $Q(\alpha) = 0.75$, 0.5, and 0.25 times its maximum value (+). (b) Uncertainties in photon-number (dashed curve) and phase (dashed-dotted curve) and their product (solid curve) for the Kerr-interferometer output state.

$$\langle(\Delta\hat{n}_{\text{out}})^2\rangle_{\min} = \langle\hat{n}_{\text{out}}\rangle^{1/3}, \tag{2.16}$$

where $\langle\hat{n}_{\text{out}}\rangle = \langle\hat{n}_{\text{in}}\rangle + |\xi|^2$. The minimum photon-number noise [Eq. (2.16)] is smaller than the minimum value $\langle(\Delta\hat{n}^2)\rangle_{\text{SS,min}} = \langle\hat{n}\rangle^{2/3}$ achievable by a SS. The normalized phase noise $\langle(\Delta\hat{\phi}_{\text{out}})^2\rangle/\langle\hat{n}_{\text{out}}\rangle$ is also plotted in Fig. 3(b). The phase noise is increased above the SQL because of self-phase modulation. As shown in this figure, the uncertainty product of the photon number and phase still remains the minimum value 1/4, unless γ surpasses the optimum value γ_1. That is, the output state is a NUS, yet the photon-number noise cannot be reduced below $\langle\hat{n}_{\text{out}}\rangle^{1/3}$.

The state generated by the unitary evolution [Eq. (2.13)] is not an eigenstate (Jackiw state) of the operator $e^r\hat{n} + ie^{-r}\hat{S}$ discussed in Section 1. However, the Q representation of the density operator is squeezed to a *crescent* shape by this unitary evolution, as shown in Fig. 3(a), and it resembles the mathematically constructed Jackiw state shown in Fig. 1(d).

An optical Kerr medium realizes the self-phase modulation [Eq. (2.9)], and a Mach–Zehnder interferometer with a low-reflectivity mirror ($R_2 \cong 0$) approximately achieves the unitary displacement operation [Eq. (2.11)].[29] This configuration resembles the experimental setup employed in Refs. 15 and 17. If we consider only the pump wave at frequency ω_p and the two sideband modes at $\omega_p + \Delta\omega$ and $\omega_p - \Delta\omega$, a quadratic Hamiltonian similar to Eq. (2.1) can be derived:

$$H_I = \frac{\hbar}{2}(\chi'\hat{a}_+{}^\dagger\hat{a}_-{}^\dagger + \chi'^*\hat{a}_+\hat{a}_-), \tag{2.17}$$

where $\hat{a}_+$ and $\hat{a}_-$ correspond to the upper and lower sideband modes, respectively. In reality, however, all higher-order sidebands at $\omega_p \pm n\Delta\omega$ ($n = 1, 2, \ldots$) also establish a quantum correlation with one another. This is analogous to the mutually correlated sidebands for a classical phase-modulated signal.

3. NONUNITARY STATE REDUCTION BY MEASUREMENTS OF THE FIRST KIND

A quantum measurement of the first kind is a measurement that does not destroy the measured quantum state.[30] The state immediately after a measurement of the first kind is reduced to the new state calculated by von Neumann's projection postulate.[31] In most measurement schemes, the signal state is either destroyed or becomes completely unpredictable after measurement. These are then referred to as a second-kind measurement.[30]

This section discusses the *nonunitary state reduction* by two different first-kind measurement schemes, which can produce a NUS and number states.

In a QND measurement,[32,33] for instance, of photon number, the measurement error Δn of photon number is zero, while the signal photon number is preserved. Repeated QND measurements on the same signal state do not alter the photon number. This can be considered a generation process of number states.

In a practical QND measurement of photon number, however, there are the finite measurement error Δn of the photon number and the backaction noise $\Delta\phi$ imposed upon the signal phase. These satisfy the minimum-uncertainty product $\Delta n^2 \cdot \Delta\phi^2 \cong 1/4$.[20] The result suggests intuitively that the signal quantum state after such a QND measurement is a NUS with the photon-number uncertainty determined by measurement error Δn and the sine-operator uncertainty determined by the backaction noise $\Delta\phi$.

In a parametric amplifier with no input signal and idler waves (with only incident vacuum fields), there exists a complete correlation between the output signal and idler photon numbers because of the operator Manley–Rowe relation.[21] Whenever the idler photon number is measured to be n_i, the signal photon number n_s is also equal to n_i. This can also be considered number-state generation.

In a parametric amplifier with an input signal wave in a CS, there will still be some quantum-mechanical correlation between the output signal and the idler photons. The uncertainty of the signal and idler photon numbers on the condition that the idler photon number be counted is approximately equal to one half of the photon-number noise $\langle(\Delta n_s)^2\rangle = \langle\hat{n}_s\rangle$ of the input signal wave. On the other hand, the phase noise $\langle(\Delta\phi_s)^2 = 1/4\langle n_s\rangle$ of the input signal wave is amplified by a factor of 2 after parametric amplification. This consideration intuitively suggests that the signal quantum state after a measurement of the idler photon number is a near NUS, with the photon-number uncertainty approximately determined by $\frac{1}{2}\langle(\Delta n_s)^2\rangle$ and the sine-operator uncertainty determined by $2\langle(\Delta\phi_s)^2\rangle$.

A. Quantum-Nondemolition Photon-Number Measurement

The QND measurement scheme is depicted in Fig. 4. The first stage of the measurement establishes a quantum-mechanical correlation between the signal photon number and the probe phase. It is achieved by a unitary interphase modulation produced by an optical Kerr medium. The second stage is a nonunitary reduction of the signal state. It is realized by homodyne detection of the quadrature-phase component of the probe wave.

Suppose that the signal and probe waves are initially in a CS, $|\alpha_0\rangle_a$ and $|\beta_0\rangle_b$. The initial density operator of the total system is

$$\hat{\rho}_0 = |\alpha_0\rangle_{a\,a}\langle\alpha_0|\otimes|\beta_0\rangle_{b\,b}\langle\beta_0|. \tag{3.1}$$

The interaction Hamiltonian for interphase modulation is expressed by [20,34]

$$H_I = \hbar\chi\hat{n}_a\hat{n}_b, \tag{3.2}$$

where $\hat{n}_a = \hat{a}^\dagger\hat{a}$ and $\hat{n}_b = \hat{b}^\dagger\hat{b}$ are the photon-number operators of the signal and probe waves, respectively. The unitary translation operator for this interphase-modulation process is described by

$$U = \exp(i\mu\hat{n}_a\hat{n}_b), \tag{3.3}$$

where $\mu = \chi L/v$ is the nonlinear interaction parameter, v the velocity of light in the Kerr medium, and L the interaction

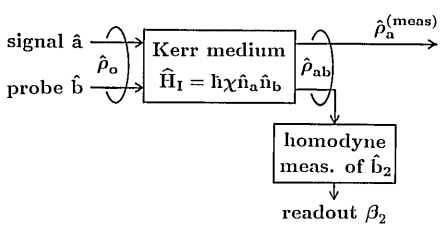

Fig. 4. Photon-number QND measurement scheme.

length. The density operator for the total system after the interphase modulation can be expressed as

$$\hat{\rho}_{ab} \equiv U\hat{\rho}_0 U^\dagger = \exp(i\mu\hat{n}_a\hat{n}_b)\hat{\rho}_0 \exp(-i\mu\hat{n}_a\hat{n}_b). \tag{3.4}$$

The signal wave after this first stage experiences an increase in phase uncertainty but still features Poissonian photon statistics. This can be shown by the Q representation and the photon-number distribution of the signal's reduced density operator $\hat{\rho}_a$:

$$Q_a(\alpha) \equiv {}_a\langle\alpha|\hat{\rho}_a|\alpha\rangle_a = \sum_n P_b(n)\exp(-|\alpha - \alpha_0 e^{i\mu n}|^2) \tag{3.5}$$

and

$$P_a(n) \equiv {}_a\langle n|\hat{\rho}_a|n\rangle_a = \exp(-n_a){n_a}^n/n! \quad \text{(Poisson)}, \tag{3.6}$$

where

$$\hat{\rho}_a \equiv \mathrm{Tr}_b\, \hat{\rho}_{ab} = \sum_n P_b(n)|\alpha_0 e^{i\mu n}\rangle\langle\alpha_0 e^{i\mu n}|. \tag{3.7}$$

Here $P_b(n) = \exp(-n_b){n_b}^n/n!$ is the initial Poissonian photon-number distribution of the probe wave and $n_a \equiv |\alpha_0|^2$ and $n_b \equiv |\beta_0|^2$ are initial mean photon numbers.

The signal state after the homodyne measurement of the probe-wave quadrature component $\hat{b}_2$ is given by the projection onto the eigenstate $|\beta_2\rangle_b$,[31] where β_2 is the readout of the measurement. The density operator $\hat{\rho}_a^{(\mathrm{meas})}$ after this second stage is written as

$$\hat{\rho}_a^{(\mathrm{meas})} = N\mathrm{Tr}_b(|\beta_2\rangle_{bb}\langle\beta_2|\hat{\rho}_{ab}), \tag{3.8}$$

where N is a normalization constant determined by $\mathrm{Tr}_a\, \hat{\rho}_a^{(\mathrm{meas})} = 1$. The signal photon-number distribution is modified to

$$P_a^{(\mathrm{meas})}(n) \equiv {}_a\langle n|\hat{\rho}_a^{(\mathrm{meas})}|n\rangle_a = P_a(n)G(n), \tag{3.9}$$

where

$$G(n) = N|{}_b\langle\beta_2|\beta_0 e^{i\mu n}\rangle_b|^2 = N' \times \exp\{-2[\beta_0 \sin(\mu n - n_a \sin\mu) - \beta_2]^2\}. \tag{3.10}$$

Here $\beta_0 = |\beta_0| \exp(-in_a \sin\mu)$ is chosen so that the most probable readout from the homodyne detection is $\beta_2 = 0$. In practice, this choice of the initial probe phase is realized by adjusting the local-oscillator phase in the homodyne measurement of $\hat{b}_2$. When μ is steadily increased from zero, the photon-number distribution variance is initially decreased, but eventually it increases again. This is because the modification factor $G(n)$ is a multiple-peaked function of n with the peak interval π/μ as indicated by Eq. (3.10). When μ is larger, sidelobes emerge in the photon-number distribution, increasing its variance.[34] To avoid the sidelobes in $P_a^{(\mathrm{meas})}(n)$, the interval π/μ should be greater than the initial photon-number uncertainty α_0:

$$\mu \ll \pi/|\alpha_0|. \tag{3.11}$$

For such weak nonlinear interaction, $G(n)$ is approximated by the Gaussian function

$$G(n) \cong N' \exp\{-2[|\beta_0|\mu(n - n_a) - \beta_2]^2\}, \tag{3.12}$$

where N' is a normalization constant. $P_a(n)$ can also be approximated by a Gaussian with variance $\langle(\Delta n_a)^2\rangle = n_a$ when $n_a \gg 1$. Therefore $P_a^{(\mathrm{meas})}(n)$ can be rewritten as

$$P_a^{(\mathrm{meas})}(n) \cong N'' \exp[-(n - n_a - \sqrt{2}\beta_2)^2/2\langle(\Delta\hat{n})^2\rangle]. \tag{3.13}$$

This is the conditional probability of finding n photons in the signal given that β_2 was measured in the homodyne measurement. The conditional photon-number noise is

$$\langle(\Delta\hat{n})^2\rangle = \left(\frac{1}{n_a} + 4\mu^2 n_b\right)^{-1}. \tag{3.14}$$

Note that $1/4\mu^2 n_b$ is the error of the QND photon-number measurement. The signal photon-number noise can be decreased to an arbitrarily low level by increasing the probe photon number n_b because expression (3.11) does not constrain n_b in any way. As an alternative way to decrease $\langle\Delta\hat{n}^2\rangle$, we can use a phase SS for the probe wave.

The signal phase uncertainty is not affected at all by the $\hat{b}_2$ measurement. The sine-operator uncertainty is calculated from $\hat{\rho}_a$ as

$$\langle(\Delta\hat{S})^2\rangle \cong \frac{1}{4n_a} + [1 - \exp(-2\mu^2 n_b)]/2. \tag{3.15}$$

The second term is the increase of phase uncertainty by interphase modulation and can be regarded as the backaction noise of the QND measurement. The square of the cosine-operator mean is also calculated as

$$\langle\hat{C}\rangle^2 \cong \exp(-\mu^2 n_b). \tag{3.16}$$

The normalized number-phase uncertainty product is thus given by

$$P_{nS} \equiv \frac{\langle(\Delta\hat{n})^2\rangle\langle(\Delta\hat{S})^2\rangle}{\langle\hat{C}\rangle^2} \cong \frac{1}{4}\sinh(\mu^2 n_b)/(\mu^2 n_b). \tag{3.17}$$

Even when $\mu^2 n_b$ is increased to 1/4 to achieve $\langle(\Delta\hat{n})^2\rangle \leqq 1$ (near number state), the uncertainty product is still close to the minimum value of 1/4. The Fano factor $F = \langle(\Delta\hat{n})^2\rangle/\langle\hat{n}\rangle$, the sine-operator uncertainty $\langle(\Delta\hat{S})^2\rangle$, the square of the cosine-operator mean $\langle\hat{C}\rangle^2$, and the normalized number-phase uncertainty product P_{nS} numerically calculated using $\hat{\rho}_a^{(\mathrm{meas})}$ in Eq. (3.8) are plotted as functions of μ in Fig. 5.

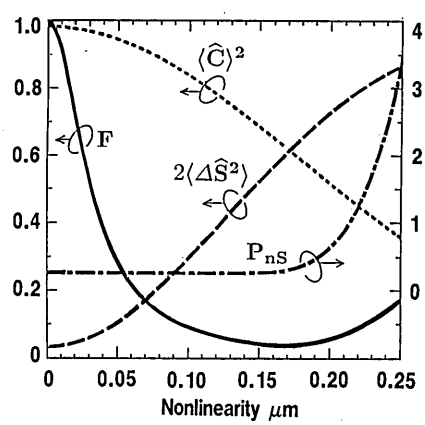

Fig. 5. Fano factor F (solid curve), sine uncertainty (dashed curve), square of cosine mean (dotted curve), and number-phase uncertainty product P_{ns} (dashed–dotted curve) of the state after readout $\beta_2 = 0$ numerically calculated from $\hat{\rho}_a^{(\mathrm{meas})}$.

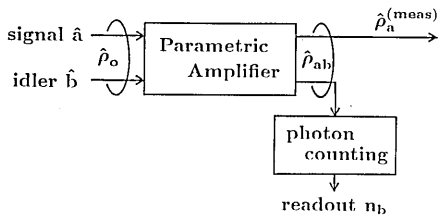

Fig. 6. Parametric amplifier with idler photon counting.

B. Parametrically Amplified Idler Photon Counting

A parametric amplifier with an idler photon-counting measurement is depicted in Fig. 6. The first stage of this scheme is also an establishment of the quantum-mechanical correlation between the signal and idler waves. It is achieved by the unitary parametric interaction in the second-order nonlinear medium. The second stage is a nonunitary reduction of the signal quantum state, which is realized by an idler photon-counting measurement.

Suppose that the signal and idler waves are initially in a CS, $|\alpha_0\rangle_a$, and in a vacuum state, $|0\rangle_b$, respectively. The initial density operator of the total system is

$$\hat{\rho}_0 = |\alpha_0\rangle_{aa}\langle\alpha_0| \otimes |0\rangle_{bb}\langle 0|. \tag{3.18}$$

The interaction Hamiltonian for nondegenerate parametric interaction is expressed by

$$H_I = \frac{\hbar}{2}(\chi \hat{a}^\dagger \hat{b}^\dagger + \chi^* \hat{a}\hat{b}), \tag{3.19}$$

where $\hat{a}$ and $\hat{b}$ are the annihilation operators of the signal and idler waves. The unitary translation operator for the parametric interaction is

$$\begin{aligned} U &= \exp[i\eta(\hat{a}^\dagger b^\dagger + \hat{a}\hat{b})] \\ &= \frac{1}{\cosh\eta} \exp[i(\tanh\eta)\hat{a}^\dagger b^\dagger] \exp[-\ln(\cosh\eta)\hat{a}^\dagger\hat{a}] \\ &\quad \times \exp[-\ln(\cosh\eta)\hat{b}^\dagger\hat{b}] \exp[i(\tanh\eta)\hat{a}\hat{b}], \end{aligned} \tag{3.20}$$

where $\eta = \chi L/v$. The density operator for the total system after the parametric amplification is then given by

$$\begin{aligned} \hat{\rho}_{ab} \equiv U\hat{\rho}_0 U^\dagger = \frac{1}{\cosh^2\eta} &\exp[i(\tanh\eta)\hat{a}^\dagger b^\dagger] \\ &\times \exp[-\ln(\cosh\eta)\hat{a}^\dagger\hat{a}] \\ &\times \hat{\rho}_0 \exp[-\ln(\cosh\eta)\hat{a}^\dagger\hat{a}] \\ &\times \exp[-i(\tanh\eta)\hat{a}\hat{b}]. \end{aligned} \tag{3.21}$$

The output-signal mean photon number is amplified to

$$\langle \hat{n}_a \rangle \cong |\alpha_0|^2 \cosh^2\eta, \tag{3.22}$$

where $|\alpha_0|^2 \gg 1$ is assumed. The number and sine-operator uncertainties are

$$\langle \Delta\hat{n}_a{}^2 \rangle \cong \langle \hat{n}_a \rangle (2\sinh^2\eta + 1), \tag{3.23a}$$

$$\langle \Delta\hat{S}_a{}^2 \rangle \cong \frac{1}{4\langle \hat{n}_a \rangle}(2\sin^2\eta + 1). \tag{3.23b}$$

These are thus both much larger than the SQL. The idler photon-number distribution is peaked around its mean value,

$$\langle \hat{n}_b \rangle \cong |\alpha_0|^2 \sinh^2\eta. \tag{3.24}$$

The signal quantum state after the idler photon-counting measurement is given by the projection onto the photon-number eigenstate $|n_b\rangle_b$, where n_b is the detected number of idler photons. The density operator $\hat{\rho}_a{}^{(\mathrm{meas})}$ after this second stage is written as

$$\hat{\rho}_a{}^{(\mathrm{meas})} = N \,\mathrm{Tr}_b\,(|n_b\rangle_{bb}\langle n_b|\hat{\rho}_{ab}), \tag{3.25}$$

where N is a normalization constant determined by $\mathrm{Tr}_a\,\hat{\rho}_a{}^{(\mathrm{meas})} = 1$. The signal photon-number distribution is calculated from Eq. (3.21) as

$$P_a{}^{(\mathrm{meas})}(n) = \begin{cases} N \exp(-|\alpha_0 \tanh\eta|^2) \binom{n}{n_b} \dfrac{(\tanh^2\eta)^{n_b}}{\cosh^2\eta} \exp(-|\alpha_0\cosh\eta|^2) \dfrac{|\alpha_0\cosh\eta|^{2(n-n_b)}}{(n-n_b)!} & (\text{for } n \geqq n_b) \\ 0 & (\text{for } n < n_b) \end{cases}, \tag{3.26}$$

where $\binom{n}{n_b}$ is a binomial coefficient.

The mean and the variance of the signal photon number, sine uncertainty, and uncertainty product P_{nS}, on the condition that n_b be measured and its most probable value found, are numerically calculated by using Eq. (3.25) and are shown in Fig. 7.

The results ensure that $\langle(\Delta\hat{n})^2\rangle \to \frac{1}{2}|\alpha_0|^2$ for large η and that the sine-operator uncertainty is well approximated by expression (3.23b). Their product remains close to the minimum value of 1/4, so the state generated by this scheme is also a NUS. The Fano factor is arbitrarily decreased with increasing nonlinear interaction η, $\langle\Delta\hat{n}^2\rangle/|\alpha_0|^2\cosh^2\eta \to 0$.

The readouts β_2 of the probe homodyne detection in a QND scheme and n_b of the idler photon-counting detection in a parametric amplifier scheme differs from one measurement to the next. Each signal state is thus reduced to a

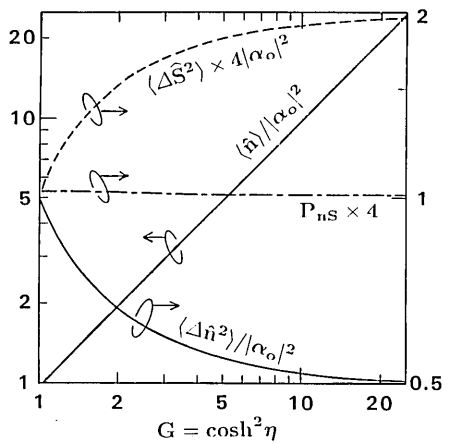

Fig. 7. Normalized photon-number mean and uncertainty (solid lines), sine uncertainty (dashed line), and uncertainty product P_{nS} (dashed–dotted line) for the signal output state on condition that the idler output number has been measured to be n_b.

different NUS after the measurement. Unfortunately, the probability of finding a prescribed β_2 or n_b decreases as the measurement error is decreased. This means that the probability of generating a NUS with a desired photon number decreases as the photon-number noise becomes smaller.

A continuous generation of the desired NUS is possible only if the deviation in β_2 or n_b from the prescribed value is eliminated by feedback control to a signal-wave generator. This possibility is discussed in Section 4.

4. MEASUREMENT-FEEDBACK COMBINATION

As was discussed in Section 3, a signal wave that is initially in a CS is reduced to a near NUS in the two described measurement schemes. However, each wave packet is reduced to a different NUS, corresponding to the different readout of each individual measurement. Thus the reduced density operator $\hat{\rho}_a = \mathrm{Tr}_b(\hat{\rho}_{ab})$, which describes the ensemble of these wave packets, does not feature sub-Poissonian photon-number distributions. A specific NUS is generated only when a certain wave packet featuring the prescribed readout is artificially selected.

In this section we demonstrate that every generated wave packet can be reduced to the same NUS when the deviation of the measurement readout from the desired value is continuously fed back to the signal-wave generator.

A. Negative-Feedback Semiconductor Laser

The feasibility of feedback control to a signal generator is studied by a negative-feedback semiconductor laser.[22] A single-frequency GaAs-laser output is directly detected by a Si photodiode. The photocurrent fluctuation is phase reversed and fed back to the laser pump current, as shown in Fig. 8(a).

The photocurrent spectral density measured by the spectrum analyzer is 4 dB higher then the shot-noise level, and the photoelectron statistics measured by an analog photon counter is super-Poissonian, with $\langle(\Delta\hat{n})^2\rangle \cong 2.8\langle\hat{n}\rangle$ for the free-running laser, as shown in Fig. 8(b). The result suggests that the signal-wave generator produces a classical mixture of CS's instead of a pure CS, under the free-running condition. The Poissonian statistics are obtained by a GaAs light-emitting diode output or a filtered incandescent light.

When the feedback loop is closed, the photocurrent spec-

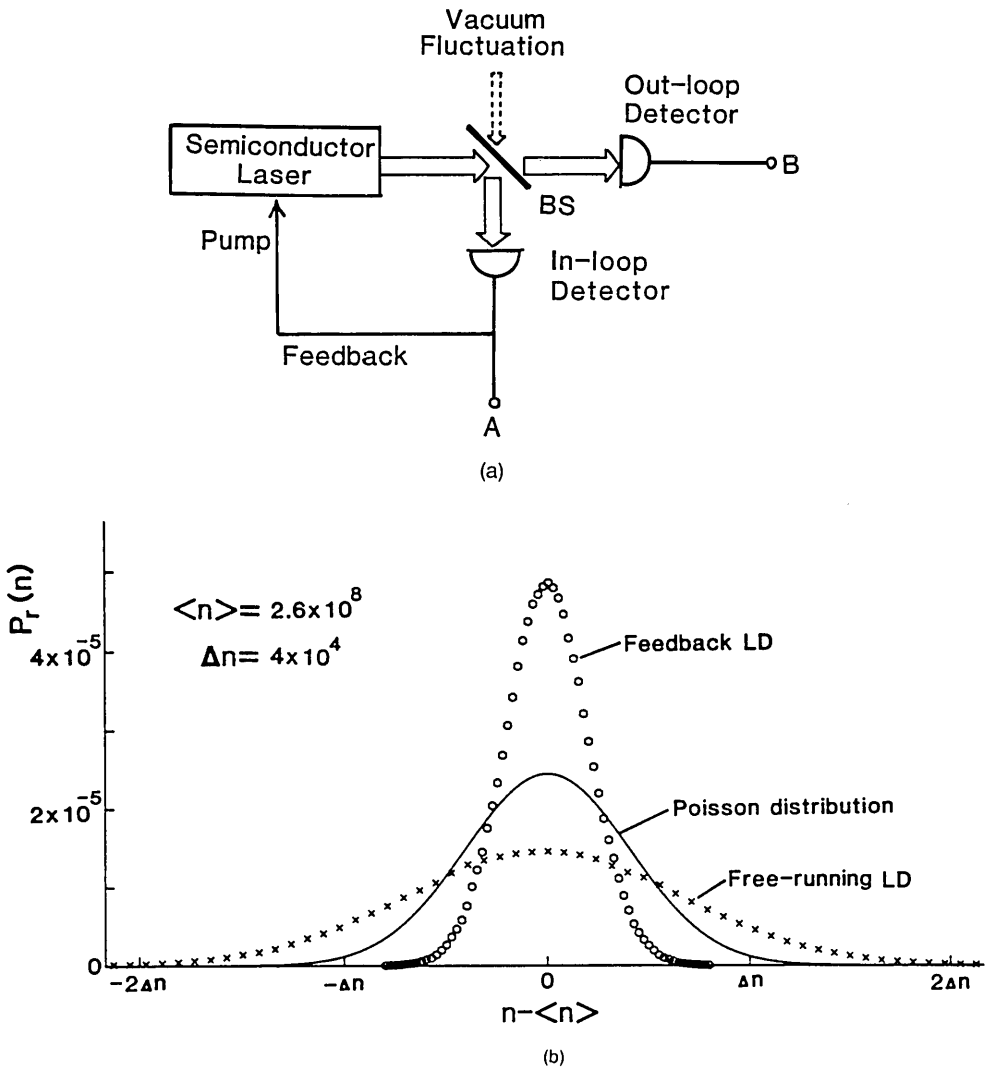

Fig. 8. (a) Experimental setup for photon-number fluctuation reduction by negative feedback. The in-loop current (terminal A) will show reduced noise below the SQL, whereas the out-loop photocurrent noise level (terminal B) will be above the SQL because of the quantum noise introduced by the 50–50 beam splitter (BS). (b) Measured photon statistics by analog photon counting.

tral density is reduced to 7 dB below the shot-noise level, and the photoelectron statistics are sub-Poissonian, with $\langle(\Delta\hat{n}^2)\rangle \cong 0.26\ \langle\hat{n}\rangle$, as shown in Fig. 8(b). It is suggested from these experimental results that feedback can control the reduction of the wave function and can produce continuous generation of a NUS.

It is, however, impossible to extract the NUS from the feedback loop in this configuration. If the laser output is divided into two parts by a beam splitter, and one part is used for feedback stabilization while the other part is used as an output wave, the photocurrent spectral density and photoelectron statistics become even worse than under the free-running condition.[22] The reason is that the vacuum field incident upon a beam splitter deteriorates the quantum-mechanical correlation between the photon numbers of the two output waves from the beam splitter. There remain subtle conceptual issues with this experiment, such as the role of state reduction by measurement and the mismatch of the modes between the in-loop photon field and the converted photocurrent pulse. Theoretical studies along these lines are now under way.[22,35,36]

In order to extract the NUS from the loop, the beam splitter must be replaced by a device that preserves the quantum-mechanical correlation between the output and reference waves. The interphase modulation in the Kerr medium[20] and the parametric interaction in the second-order nonlinear medium[23,24] thus emerge as essential parts of a measurement-feedback configuration.

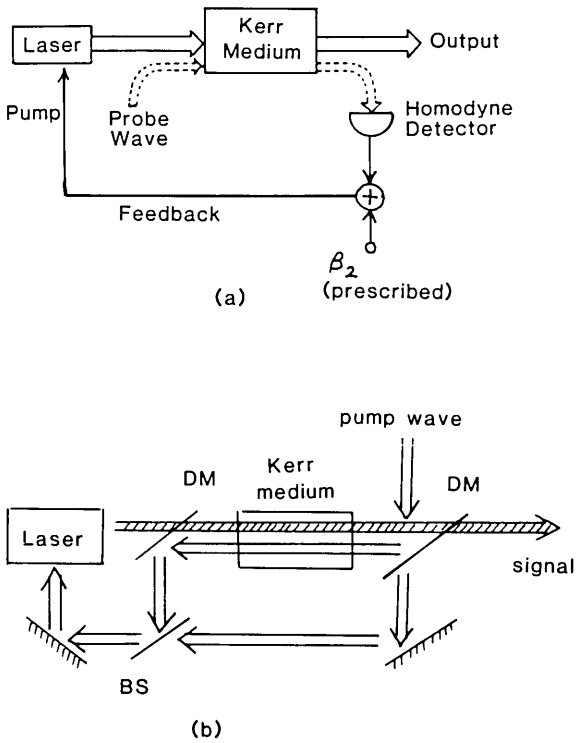

Fig. 9. (a) Basic configuration for NUS generation by using QND measurement and feedback. (b) An all-optical realization of QND measurement–feedback. DM's, dichroic mirrors; BS, beam splitter.

B. Laser Oscillator with Quantum Nondemolition Measurement-Feedback

The basic configuration of a QND measurement–feedback is shown in Fig. 9(a). The output photon flux of the laser is measured by the QND detector discussed in Subsection 3.A. The deviation from the prescribed value is phase reversed and fed back to the laser pump.

The quantum-mechanical analysis of the measurement–feedback configuration is not trivial. The usual quantum-mechanical approach is to study the unitary time evolution and the reduction of the density operator, as discussed in Sections 2 and 3. The steady-state conditions prevailing in a practical system are simulated by a succession of inputs, each followed in its time evolution to the output. Needless to say, the introduction of feedback from the output is not treated conveniently in this manner. The Heisenberg approach using Langevin-operator noise sources is convenient for this problem. The analysis can be carried out in terms of Fourier analysis of the time-dependent operator equations.

The equation of motion for the laser-cavity internal-field annihilation operator $\hat{A}$ in the slowly varying envelope approximation reads as[22]

$$\frac{\mathrm{d}}{\mathrm{d}t}\hat{A} = -\tfrac{1}{2}[\gamma_e + \gamma_o - \frac{\omega}{n_r{}^2}(\tilde{\chi}_i - i\tilde{\chi}_r)]\hat{A} + \hat{G}(t) + \sqrt{\gamma_e}\hat{f}(t). \tag{4.1}$$

Here γ_e and γ_o are the photon-decay rates that are due to output coupling and internal loss. n_r is the nonresonant refractive index, and $\tilde{\chi}_i - i\tilde{\chi}_r$ is the complex third-order nonlinear susceptibility that represents the stimulated photon gain and anomalous refractive-index dispersion. $\hat{G}(t)$ is the noise operator that accounts for the dipole fluctuation and internal loss oscillators.[37,38] $\hat{f}(t)$ is the noise operator that accounts for the vacuum-field fluctuation incident upon the cavity.[39,40] The correlation functions for the Hermitian quadrature operators for $\hat{G}$ and $\hat{f}$ are given by

$$\langle\hat{G}_1(t)\hat{G}_1(s)\rangle = \langle\hat{G}_2(t)\hat{G}_2(s)\rangle = \delta(t-s)\frac{1}{4}[\gamma_0 + (\langle\tilde{E}_{cv}\rangle + \langle\tilde{E}_{vc}\rangle)] \tag{4.2}$$

and

$$\langle\hat{f}_1(t)\hat{f}_1(s)\rangle = \langle\hat{f}_2(t)\hat{f}_2(s)\rangle = \delta(t-s)\frac{1}{4}. \tag{4.3}$$

Here $\tilde{E}_{cv}$ and $\tilde{E}_{vc}$ are the stimulated-emission and absorption-rate operators. They are related to $\tilde{\chi}_i$ by $(\omega/n^2)\tilde{\chi}_i = \tilde{E}_{cv} - \tilde{E}_{vc}$. $\tilde{\chi}_i - i\chi_i$ is dependent on the population-difference operator $\tilde{N}_c$ that obeys the following equation of motion[22]:

$$\frac{\mathrm{d}}{\mathrm{d}t}\tilde{N}_c = \tilde{P} - \frac{\tilde{N}_c}{\tau_{\mathrm{sp}}} - (\tilde{E}_{cv} - \tilde{E}_{vc})\hat{n} - \tilde{E}_{cv} + \tilde{F}_c(t). \tag{4.4}$$

Here $\tilde{P}$ is the pump-rate operator that includes the feedback term, τ_{sp} is the spontaneous-emission lifetime, and $\tilde{F}_c$ is the Hermitian noise operator that accounts for the pump fluctuation and fluctuation in spontaneous emission, stimulated emission, and absorption. The correlation function of $\tilde{F}_c$ can be written as

$$\langle\tilde{F}_c(t)\tilde{F}_c(s)\rangle = \delta(t-s)\left[\langle\tilde{P}\rangle + \frac{\langle\tilde{N}_c\rangle}{\tau_{\mathrm{sp}}} + (\langle\tilde{E}_{cv}\rangle + \langle\tilde{E}_{vc}\rangle)\langle\hat{n}\rangle\right]. \tag{4.5}$$

The first term in Eq. (4.5) represents the shot-noise character of the pump process. The pump-rate operator $\tilde{P}$ does not include this noise term but retains the feedback control signal that will be derived below. $\hat{G}_1(t)$ and $\tilde{F}_c(t)$ share the same noise source, i.e., the dipole fluctuation, so they are partly correlated:

$$\langle \tilde{F}_c(t)\hat{G}_1(s)\rangle = -\delta(t-s)\frac{1}{2}\langle \hat{n}\rangle^{1/2}(\langle \tilde{E}_{cv}\rangle + \langle \tilde{E}_{vc}\rangle). \quad (4.6)$$

The operator $\hat{A}$ describes the discrete cavity internal mode. However, it is not a normal mode in a strict sense, because it is coupled to the continuous modes in free space through the output coupling mirrors. It is a discrete mode but a quasi-mode.[38] The physical quantity in which we are interested is not this quasi-mode inside the cavity but the output wave $\hat{r}$ emanating from the cavity. The boundary condition can be written in terms of the Fourier components of $\hat{A}$, $\hat{r}$, and $\hat{f}$ as follows[39,40]:

$$\hat{r}(\Omega) = -\hat{f}(\Omega) + \sqrt{\gamma_e}\hat{A}(\Omega). \quad (4.7)$$

A QND detector measures the photon-flux operator $\hat{N} = \hat{r}^\dagger\hat{r}$ of the output wave. The readout is compared with the prescribed value N_0, and the deviation from N_0 is fed back to adjust the pump rate. As discussed in Subsection 3.A, the readout is subject to a finite measurement error, and the feedback signal consists of the photon-flux fluctuation operator

$$\Delta\hat{N}^{(\text{meas})} = \Delta\hat{N} - \frac{\Delta\hat{\phi}_p}{\mu} = 2\langle\hat{r}\rangle\Delta\hat{r} - \frac{\Delta\hat{\phi}_p}{\mu}, \quad (4.8)$$

where $\Delta\hat{N} = \hat{N} - \langle\hat{N}\rangle \cong 2\langle\hat{r}\rangle\Delta\hat{r}$ and $\Delta\hat{\phi}_p$ is the phase noise of the probe wave. The pump-rate operator $\tilde{P}$ is now expressed as

$$\tilde{P} = \langle\tilde{P}\rangle - \int_0^\infty h(\theta)\otimes\left[2\langle\hat{r}\rangle\Delta\hat{r}(t-\theta) - \frac{\Delta\hat{\phi}_p(t-\theta)}{\mu}\right]d\theta. \quad (4.9)$$

Here $h(\theta)$ is the impulse response of the feedback loop that accounts for a loop delay and loop gain. The signal wave experiences phase modulation in the Kerr medium because of the photon-number noise $\Delta\hat{n}_p$ of the probe wave,

$$\Delta\hat{\psi} = \Delta\hat{\psi}^0 - \mu\Delta\hat{n}_p, \quad (4.10)$$

where $\Delta\hat{\psi}^0$ is the initial phase noise of the signal wave.

Solving Eqs. (4.1), (4.4), (4.7), (4.9), and (4.10) in a self-consistent manner, the spectra for the in-phase and quadrature-phase fluctuations of the output signal wave within the feedback-loop bandwidth are obtained as[22]

$$S_{\Delta\hat{r}_1}(\Omega) = \frac{1}{2}\frac{\gamma_e^2 + \Omega^2 + \dfrac{|H(\Omega)|^2\gamma_e^2}{2\mu^2\langle\hat{r}\rangle^2}S_{\Delta\hat{\phi}_p}(\Omega)}{\gamma_e^2|1+H(\Omega)|^2 + \Omega^2}$$

$$\xrightarrow[|H(\Omega)|\to\infty]{} \frac{S_{\Delta\hat{\phi}_p}(\Omega)}{4\mu^2\langle\hat{r}\rangle^2} \quad (4.11)$$

and

$$S_{\Delta\hat{r}_2}(\Omega) = \frac{\gamma_e^2}{\Omega^2} + \frac{1}{2} + \mu^2 S_{\Delta\hat{n}_p}(\Omega)\,\langle\hat{r}\rangle^2, \quad (4.12)$$

where $S_{\Delta\hat{\phi}_p}$ and $S_{\Delta\hat{n}_p}$ are the spectra of the phase-fluctuation and photon-flux fluctuation operators of the probe wave in the QND measurement.

Equation (4.11) can be rewritten in terms of the photon-flux noise spectrum as

$$S_{\Delta\hat{N}}(\Omega) \cong 4\langle\hat{r}\rangle^2 S_{\Delta\hat{r}}(\Omega) = \frac{S_{\Delta\phi_p}(\Omega)}{\mu^2}. \quad (4.13)$$

The phase-operator fluctuation spectrum $S_{\Delta\hat{\psi}}(\Omega)$ of the signal is approximately given by $S_{\Delta\hat{\psi}}(\Omega) = S_{\Delta\hat{r}2}(\Omega)/\langle\hat{r}\rangle^2$. Therefore the product of $S_{\Delta\hat{N}}(\Omega)$ and $S_{\Delta\psi}(\Omega)$ is reduced to the spectral uncertainty product of the probe wave:

$$S_{\Delta\hat{N}}(\Omega)S_{\Delta\hat{\psi}}(\Omega) = S_{\Delta\hat{n}_p}(\Omega)S_{\Delta\hat{\phi}_p}(\Omega), \quad (4.14)$$

when the first two terms in Eq. (4.12) are assumed to be negligible as compared with the third term of the backaction noise. If the probe wave is in a broadband coherent state, which approximately satisfies the number-phase spectral-density minimum-uncertainty product, the output wave will also satisfy the number-phase spectral-density minimum-uncertainty product,

$$[\hat{r}(\Omega), \hat{r}^\dagger(\Omega')] = \delta(\Omega-\Omega') \xrightarrow[\text{(Schwartz inequality)}]{} \left.\begin{aligned} S_{\Delta\hat{r}_1}(\Omega)S_{\Delta\hat{r}_2}(\Omega) &\geqq 1/4 \\ S_{\Delta\hat{N}}(\Omega)S_{\Delta\hat{\psi}}(\Omega) &\geqq 1, \end{aligned}\right\}. \quad (4.15)$$

This is the generation principle of a broadband NUS. The photon-flux spectrum can be reduced below the SQL, $S_{\Delta\hat{N}}(\Omega)_{\text{SQL}} = 2\langle\hat{N}\rangle$, and can eventually be reduced to zero by increasing the probe-wave intensity.

Experimental efforts to demonstrate the QND photon-number measurement are now under way, using an optical fiber as a Kerr medium.[41,42]

C. Nondegenerate Parametric Oscillator with Idler Measurement–Feedback

As discussed in Subsection 3.B, a parametric amplifier establishes a quantum-mechanical correlation between the signal and idler photon numbers. The operator Manley–Rowe relation reads as[13]

$$\hat{n}_s(t) - \hat{n}_i(t) = \hat{n}_s(0) - \hat{n}_i(0), \quad (4.16)$$

where $\hat{n}_s(0)$ and $\hat{n}_i(0)$ are the input photon-number operators of the signal and the idler, respectively. It suggests that the correlation is perfect when both the signal and the idler waves are initially in the vacuum state. A nondegenerate parametric oscillator is a promising device for NUS and number-state generation because it produces coherent signal and idler emission, starting from the vacuum states. The basic configuration of an idler measurement–feedback nondegenerate parametric oscillator is shown in Fig. 10(a). The cavity is assumed to be single ended and triply resonant, i.e., the signal, idler, and pump waves are all confined in the high-Q cavity. The idler-output photon flux is measured by a conventional photodetector. The deviation from the pre-

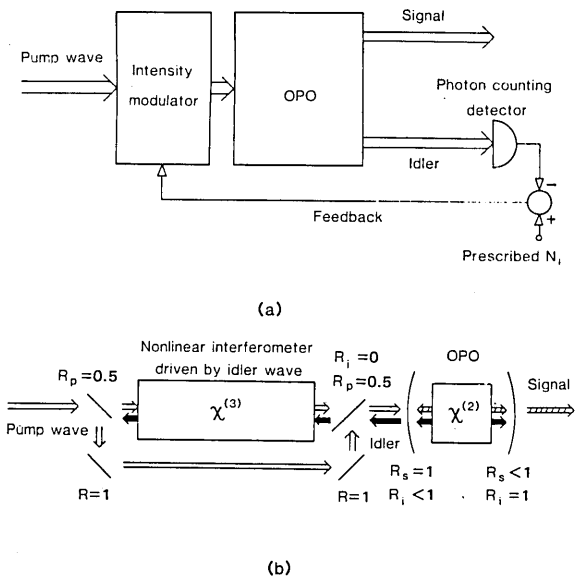

Fig. 10. (a) A nondegenerate optical parametric oscillator (OPO) with idler photon-flux measurement–feedback. The idler output photon flux is measured in a photon-counting detector and compared to some prescribed value N_i. The deviation is fed back to a pump-wave intensity modulator. (b) An all-optical realization of a nondegenerate OPO with idler photon-flux measurement–feedback. The asymmetric OPO cavity separates the idler beam (which has output to the left) from the signal (which has output to the right). The idler-beam photon flux is used to modulate the phase of the pump beam in the upper arm of a Mach–Zender interferometer using an optical Kerr medium, as described in Subsection 3.A. When the pump intensity and the lower-arm optical path length are adjusted according to the prescribed idler photon flux N_i, the interferometer will simultaneously perform idler flux measurement and pump intensity modulation.

scribed value is phase reversed and fed back to the pump-wave intensity.

The total Hamiltonian of this system is[43]

$$\begin{aligned} H &= \hbar\omega_s \hat{a}_s^\dagger \hat{a}_s + \hbar\omega_i \hat{a}_i^\dagger \hat{a}_i + \hbar\omega_p \hat{a}_p^\dagger \hat{a}_p \\ &\quad + i\hbar\chi(\hat{a}_s^\dagger \hat{a}_i^\dagger \hat{a}_p - \hat{a}_s \hat{a}_i \hat{a}_p^\dagger) \\ &\quad + i\hbar\hat{E}_p\,[\hat{a}_p^\dagger \exp(-i\omega_p t) - \hat{a}_p \exp(i\omega_p t)] \\ &\quad + i\hbar(\sqrt{\gamma_s}\hat{a}_s \hat{f}_s^\dagger + \sqrt{\gamma_i}\hat{a}_i \hat{f}_i^\dagger + \sqrt{\gamma_p}\hat{a}_p \hat{f}_p^\dagger - \text{H.c.}) \end{aligned} \tag{4.17}$$

Here $\hat{a}_s$, $\hat{a}_i$, and $\hat{a}_p$ are the cavity-internal-field annihilation operators for signal, idler, and pump waves, respectively; χ is the normalized second-order nonlinear coefficient responsible for the parametric interaction; $\hat{E}_p$ is the pump-rate operator, which includes a feedback term; γ_s is the signal photon-decay rate that is due to output coupling; and $\hat{f}_s$ is the vacuum fluctuation incident upon the output mirror. γ_i, $\hat{f}_i$, γ_p, and $\hat{f}_p$ are the corresponding quantities for the idler and pump waves. The cavity's internal loss is assumed to be negligible.

The equations of motion for the cavity-internal-field operators read as

$$\frac{d}{dt}\hat{a}_s = -\left(i\omega_s + \frac{\gamma_s}{2}\right)\hat{a}_s + \chi\hat{a}_i^\dagger \hat{a}_p + \sqrt{\gamma_s}\hat{f}_s, \tag{4.18}$$

$$\frac{d}{dt}\hat{a}_i = -\left(i\omega_i + \frac{\gamma_i}{2}\right)\hat{a}_i + \chi\hat{a}_s^\dagger \hat{a}_p + \sqrt{\gamma_i}\hat{f}_i, \tag{4.19}$$

and

$$\frac{d}{dt}\hat{a}_p = -\left(i\omega_p + \frac{\gamma_p}{2}\right)\hat{a}_p - \chi\hat{a}_s\hat{a}_i + \hat{E}_p \exp(-i\omega_p t) + \sqrt{\gamma_p}\hat{f}_p. \tag{4.20}$$

Using the rotating frame and quasi-linearization such as

$$\hat{a}_s \equiv \hat{A}_s \exp(-i\omega_s t) = (A_s + \Delta\hat{A}_{1s} + i\Delta\hat{A}_{2s}) \exp(-i\omega_s t),$$

we obtain three c-number coupled equations for the mean amplitudes and six coupled equations for the fluctuating operators:

$$\frac{\gamma_s}{2} A_s = \chi A_i^* A_p, \tag{4.21}$$

$$\frac{\gamma_i}{2} A_i = \chi A_s^* A_p, \tag{4.22}$$

$$\frac{\gamma_p}{2} A_p = \langle \hat{E}_p \rangle - \chi A_s A_i, \tag{4.23}$$

$$\frac{d}{dt}\Delta\hat{A}_{1s} = -\frac{\gamma_s}{2}\Delta\hat{A}_{1s} + \chi A_p \Delta\hat{A}_{1i} + \chi|A_i|\Delta\hat{A}_{1p} + \sqrt{\gamma_s}\hat{f}_{1s}, \tag{4.24}$$

$$\frac{d}{dt}\Delta\hat{A}_{2s} = -\frac{\gamma_s}{2}\Delta\hat{A}_{2s} - \chi A_p \Delta\hat{A}_{2i} + \chi|A_i|\Delta\hat{A}_{2p} + \sqrt{\gamma_s}\hat{f}_{2s}, \tag{4.25}$$

$$\frac{d}{dt}\Delta\hat{A}_{1i} = -\frac{\gamma_i}{2}\Delta\hat{A}_{1i} + \chi A_p \Delta\hat{A}_{1s} + \chi|A_s|\Delta\hat{A}_{1p} + \sqrt{\gamma_i}\hat{f}_{1i}, \tag{4.26}$$

$$\frac{d}{dt}\Delta\hat{A}_{2i} = -\frac{\gamma_i}{2}\Delta\hat{A}_{2i} - \chi A_p \Delta\hat{A}_{2s} + \chi|A_s|\Delta\hat{A}_{2p} + \sqrt{\gamma_i}\hat{f}_{2i}, \tag{4.27}$$

$$\begin{aligned} \frac{d}{dt}\Delta\hat{A}_{1p} &= -\frac{\gamma_p}{2}\Delta\hat{A}_{1p} - \int_0^\infty h(\theta) \otimes [\hat{E}_p(t-\theta) - \langle \hat{E}_p \rangle]\,d\theta \\ &\quad - \chi|\hat{A}_s|\Delta A_{1i} - \chi|A_i|\Delta\hat{A}_{1s} + \sqrt{\gamma_p}\hat{f}_{1p}, \end{aligned} \tag{4.28}$$

and

$$\frac{d}{dt}\Delta\hat{A}_{2p} = -\frac{\gamma_p}{2}\Delta\hat{A}_{2p} - \chi|A_s|\Delta\hat{A}_{2i} - \chi|A_i|\Delta\hat{A}_{2s} + \sqrt{\gamma_p}\hat{f}_{2p}. \tag{4.29}$$

From Eqs. (4.21)–(4.23), the mean respective photon numbers of the cavity internal signal, idler, and pump waves are given by

$$\langle \hat{n}_s \rangle \equiv |A_s|^2 = \sqrt{\gamma_i/\gamma_s}\,\frac{1}{\chi}\left(\langle \hat{E}_p \rangle - \frac{\sqrt{\gamma_i\gamma_s}\gamma_p}{4\chi}\right), \tag{4.30}$$

$$\langle \hat{n}_i \rangle \equiv |A_i|^2 = \frac{\gamma_s}{\gamma_i}\langle \hat{n}_s \rangle, \tag{4.31}$$

and

$$\langle \hat{n}_p \rangle \equiv |A_p|^2 = \frac{\gamma_s\gamma_i}{4\chi^2}. \tag{4.32}$$

The second term of Eq. (4.28) represents the feedback term. The deviation of the output idler photon flux is written as

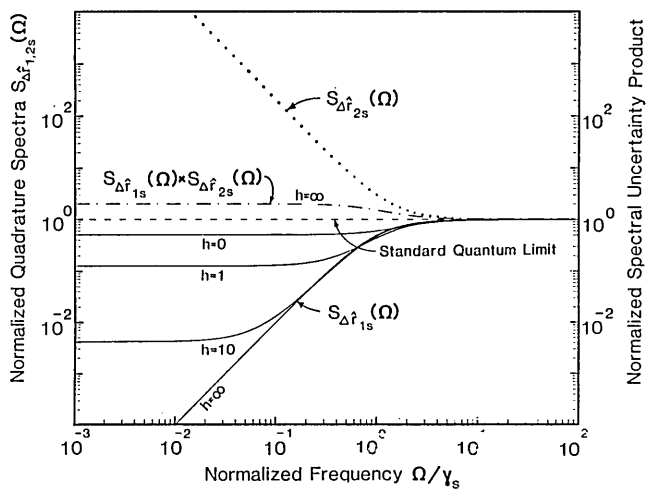

Fig. 11. The normalized in-phase (solid lines) and quadrature-phase (dotted line) signal fluctuation spectra as a function of the frequency normalized to the signal cavity decay rate γ_s. The idler and pump cavity decay rates are assumed to be much higher than γ_s, and the pump-beam intensity is much higher than the threshold level. As can be seen in the figure, the quadrature-phase fluctuations are independent of the feedback loop gain h. But below the cavity bandwidth the in-phase component fluctuations are decreased with increasing feedback gain. It should be noticed that the in-phase component is actually squeezed by 3 dB in the free-running condition ($h \equiv 0$). Above the signal bandwidth both quadrature spectra become flat and equal to the SQL. Also shown is the normalized spectral uncertainty product (dashed–dotted curve).

$$\Delta\hat{N}_i \cong 2\langle\hat{r}_i\rangle\Delta\hat{r}_{1i} = 2\sqrt{\gamma_i}|A_i|(-\hat{f}_{1i} + \sqrt{\gamma_i}\Delta\hat{A}_{1i}), \tag{4.33}$$

where N_i is the prescribed idler photon flux and the boundary condition at the output mirror Eq. (4.7) has been used. When $\langle\hat{N}_i\rangle = \gamma_i\langle\hat{n}_i\rangle$ is equal to N_i, the feedback term becomes

$$\hat{E}_p(t-\theta) - \langle\hat{E}_p\rangle = 2\gamma_i|A_i|\Delta\hat{A}_{1i}(t-\theta) - 2\sqrt{\gamma_i}|A_i|\hat{f}_{1i}(t-\theta). \tag{4.34}$$

The Fourier-transformed in-phase and quadrature fluctuation components of the output signal wave are given by

$$\Delta\hat{r}_{1s}(\Omega) = -\hat{f}_{1s}(\Omega) + \sqrt{\gamma_s}\Delta\hat{A}_{1s}(\Omega) \tag{4.35}$$

and

$$\Delta\hat{r}_{2s}(\Omega) = -\hat{f}_{2s}(\Omega) + \sqrt{\gamma_s}\Delta\hat{A}_{2s}(\Omega). \tag{4.36}$$

The spectra for $\Delta\hat{r}_{1s}$ and $\Delta\hat{r}_{2s}$ are obtained by solving Eqs. (4.24)–(4.29) and (4.34)–(4.36) in a self-consistent manner. Figure 11 shows the spectrum of the in-phase component $S_{\Delta\hat{r}_{1s}}(\Omega)$, within the feedback-loop bandwidth and at high pumping rate, as a function of the feedback gain H ($\Omega \cong 0$). The in-phase spectrum corresponds to the photon-flux fluctuation spectrum by

$$S_{\Delta\hat{N}_s}(\Omega) = 4\langle\hat{r}_s\rangle^2 S_{\Delta\hat{r}_{1s}}(\Omega).$$

With sufficiently large loop gain and for the case $\gamma_p, \gamma_i \gg \gamma_s$ (singly resonant cavity), $S_{\Delta\hat{r}_{1s}}(\Omega)$ is reduced to

$$S_{\Delta\hat{r}_{1s}}(\Omega) = \frac{1}{2}\frac{\Omega^2}{\Omega^2 + \gamma_s^2}. \tag{4.37}$$

The spectrum of the quadrature component is, on the other hand, independent of the feedback gain and features phase-diffusion noise characteristics,

$$S_{\Delta\hat{r}_{2s}}(\Omega) = \frac{1}{2}\frac{\Omega^2 + 2\gamma_s^2}{\Omega^2}. \tag{4.38}$$

Equations (4.37) and (4.38) show that the output of the idler measurement–feedback nondegenerate parametric oscillator is a near NUS with reduced photon-number noise when $\Omega \leqq \gamma_s$. The uncertainty product is, however, doubled. In the low-frequency limit, $\Omega \ll \gamma_s$, the output approaches a number state.

One practical difficulty in the measurement–feedback schemes is the delay time τ of the feedback loop. The noise is reduced only within the bandwidth determined by the loop delay

$$\Omega \leqq \pi/\tau. \tag{4.39}$$

The optical homodyne detection in the QND scheme and the photon-counting detection in the parametric scheme are not suitable for minimizing τ and realizing a broadband noise reduction. As shown in Figs. 9(b) and 10(b), τ can be minimized if the pump intensity is directly countermodulated by the probe or the idler photon flux.

5. PUMP-NOISE-SUPPRESSED LASER OSCILLATOR

In general, the macroscopic quantum coherence and fluctuation established through second-order phase transitions are determined by the balance between the system's ordering force and the reservoir's fluctuating forces. In the case of a laser oscillator, the ordering force originates from the dipole interaction between the population difference and the photon field, i.e., the gain saturation. The dominant fluctuating forces are, on the other hand, the shot-noise-limited pump-amplitude fluctuation and the zero-point fluctuation incident upon the output mirror. The dipole-moment fluctuation is suppressed at high pump levels.

That a coherent state is generated in a highly saturated laser oscillator is the consequence of the incidental balance between the two counteracting forces. If the balance can artificially be broken so that either the ordering force is enhanced or the fluctuating forces are suppressed, the laser could generate a photon field with reduced photon-number noise. In fact, the negative-feedback oscillator discussed in Section 4 can be considered an oscillator in which the above balance is favorably broken by introducing an artificial ordering force. In this section we discuss another possibility of breaking the balance by suppressing the reservoirs' fluctuating forces.

A. Origins of the Standard Quantum Limit of an Ordinary Laser Oscillator

The output-field-amplitude spectra of a free-running laser oscillator are calculated from Eqs. (4.1), (4.4), and (4.7) with the feedback parameter $h = 0$ as[22]

$$S_{\Delta\hat{P}}(\Omega) = \Big\{\gamma_e A_3{}^2[\langle\tilde{p}\rangle + \frac{\langle\tilde{N}_c\rangle}{\tau_{sp}} + (\langle\tilde{E}_{cv}\rangle + \langle\tilde{E}_{vc}\rangle)\langle\hat{n}\rangle]$$
$$+ \gamma_e(A_1{}^2 + \Omega^2)\frac{1}{4}[(\gamma_0 + \gamma_e) + (\langle\tilde{E}_{cv}\rangle + \langle\tilde{E}_{cv}\rangle)]$$
$$+ \frac{1}{4}[\gamma_e A_1 - A_2 A_3 - \Omega^2)^2 + \Omega^2(\gamma_e + A_1)^2]$$
$$+ \gamma_e A_1 A_3(\langle\tilde{E}_{cv}\rangle + \langle\tilde{E}_{vc}\rangle)\langle\hat{n}\rangle^{1/2}\Big\}$$
$$\times [(A_2{}^2 A_3{}^2 + \Omega^2)^2 + A_1{}^2\Omega^2]^{-1}. \quad (5.1)$$

Here the parameters $A_1 \sim A_3$ are defined by

$$A_1 = \frac{1}{\tau_{sp}} + \frac{1}{\tau_{st}}, \quad (5.2)$$

$$A_2 = 2(\gamma_e + \gamma_0)\langle\hat{n}\rangle^{1/2}, \quad (5.3)$$

and

$$A_3 = \frac{1}{2\langle\hat{n}\rangle^{1/2}\tau_{st}}, \quad (5.4)$$

where $\tau_{st} = \tau_{sp}/[n_{sp}(P/P_{th} - 1)]$ is the population-difference lifetime that is due to stimulated emission, $n_{sp} = \langle\tilde{E}_{cv}\rangle/(\langle\tilde{E}_{cv}\rangle - \langle\tilde{E}_{vc}\rangle)$ is a population-inversion parameter, and P_{th} is the threshold pump rate.

The output-field-amplitude noise spectrum approaches the SQL at a high pump level $P/P_{th} \gg 1$, as shown in Fig. 12(a). Also, as indicated in Fig. 12(a), the low-frequency noise at $P/P_{th} \gg 1$ below the cavity bandwidth $\Omega \leqq \gamma_e$ (near-cavity resonance) stems from the shot-noise-limited pump-amplitude fluctuation, and the high-frequency noise at $P/P_{th} \gg 1$ above the cavity bandwidth $\Omega \geqq \gamma_e$ (off-cavity resonance) originates from the vacuum fluctuation incident upon and reflected back from the output mirror.

Therefore, if the pump-amplitude fluctuation is suppressed below the ordinary shot-noise limit, the laser-amplitude noise is reduced below the SQL at $\Omega \leqq \gamma_e$, as shown in Fig. 12(b). Since the laser oscillator does not possess any restoring force against random phase walk, the phase noise spectrum always features large excess noise at $\Omega \leqq \gamma_e$. This can also be seen in Fig. 12(b). Thus the uncertainty relationship between photon-number and phase-noise spectra [Eq. (4.15)] is not violated. In fact, both the cavity internal field and the output field satisfy the commutator bracket relation, even with the pump-amplitude fluctuation term suppressed.[25]

The output-field-amplitude noise spectrum is reduced to

$$S_{\Delta\hat{P}}(\Omega) = \frac{1}{2}\frac{\Omega^2}{\Omega^2 + \gamma_e{}^2} \quad (5.5)$$

at $P/P_{th} \gg 1$ and for $\gamma_e \gg \gamma_0$ when the pump-amplitude noise is completely suppressed. The output-field phase-noise spectrum is

$$S_{\Delta\hat{\psi}}(\Omega) = \frac{1}{\langle\hat{r}\rangle^2}\left(\frac{1}{2} + \frac{\gamma_e{}^2}{\Omega^2}\right), \quad (5.6)$$

when the laser is free from anomalous dispersion and has an ideal population inversion $n_{sp} = 1$. Equations (5.5) and (5.6) suggest that the pump-noise-suppressed laser generates a CS, satisfying $S_{\Delta\hat{N}}(\Omega)S_{\Delta\hat{\psi}}(\Omega) = 1$ at $\Omega \geqq \gamma_e$, but it produces a near NUS, satisfying $S_{\Delta\hat{N}}(\Omega)S_{\Delta\hat{\psi}}(\Omega) = 2$ for frequencies be-

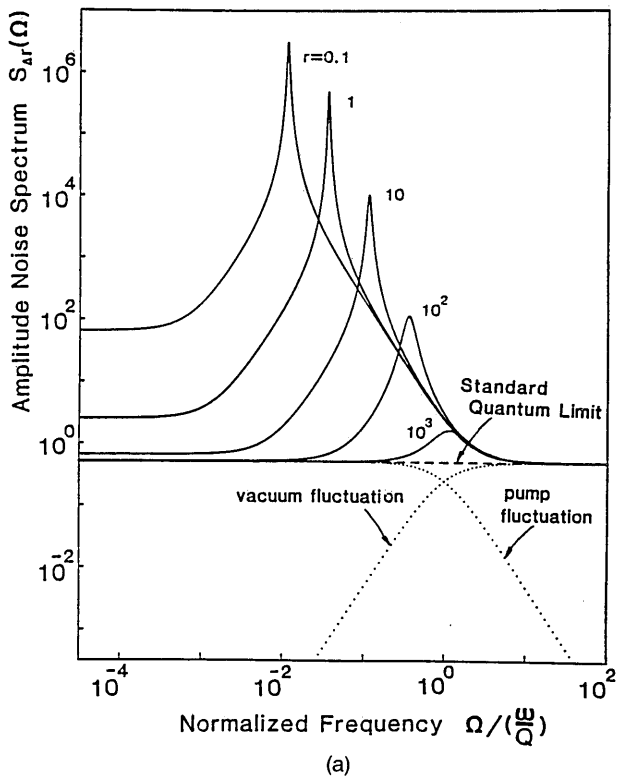

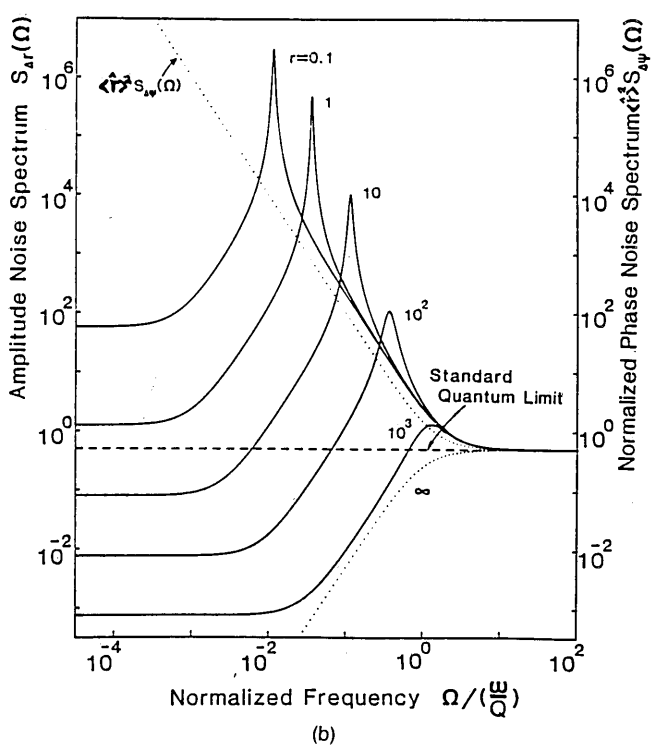

Fig. 12. (a) Amplitude noise spectra for various pump levels, $r = I/I_{th} - 1$, in an ordinary laser with shot-noise-limited pump-amplitude fluctuation. The origins for its SQL limited output at $r = \infty$ is indicated. (b) Amplitude and phase noise spectra in a pump-noise-suppressed laser.

low the cavity bandwidth. The uncertainty product is twice as large as the minimum value, similar to the near NUS generation by the parametric oscillator with idler measurement feedback, discussed in Subsection 4.C.

B. High-Impedance Suppression of Pump Fluctuation in Semiconductor Lasers

A conventional optically pumped laser oscillator has shot-noise-limited pump-amplitude fluctuation, because a pump wave, such as an incandescent light or another laser emission, features full shot noise. However, the pump-amplitude fluctuation can, in principle, be reduced below the shot-noise level without violating the fluctuation–dissipation theorem if the pump phase noise can be sacrificed. An optical pump process in a laser is a photon-counting process, so the phase noise of the pump wave does not affect the laser operation at all. However, the obvious solution for pump-amplitude noise suppression, which is optical pumping of the laser by number states, is apparently irrelevant for the present purpose.

One of the most promising schemes for pump-amplitude noise suppression is the so-called high-impedance suppression of the pump current noise in semiconductor lasers.[25,26] The junction voltage modulation in a depletion layer caused by the voltage drop across the source resistance R_s regulates the minority carrier-injection process into the active layer. The principle is analogous to the sub-Poissonian electrons produced in a space-charge-limited vacuum tube.[44]

A quantum-mechanical analysis of such a semiconductor laser must take into account the fluctuations in minority and majority carrier-transport processes and the mutual coupling between the junction current (pump source) and the junction voltage (population difference, quasi-Fermi level separation).

The microscopic theoretical analysis is summarized by the noise equivalent circuit shown in Fig. 13. R and C denote the differential resistance and the diffusion capacitance of a junction:

$$R \equiv \left(\frac{dI}{dV}\right)^{-1} = \frac{mV_T}{qN_c}\left(\frac{1}{\tau_{sp}} + \frac{1}{\tau_{st}}\right)^{-1} \tag{5.7}$$

and

$$C \equiv \frac{d(qN_c)}{dV} = \frac{qN_c}{mV_T}. \tag{5.8}$$

Here I is the average junction current, V the average junction voltage, $V_T = (k_BT)/q$ the thermal voltage, q the electron charge, and N_c the average total minority carrier number in an active volume. The constant m depends on the junction current and is usually between one and two.[45]

The current-noise source i represents the generation and recombination events of minority carriers, and its low-frequency spectrum is given by

$$S_i(\Omega) \sim 2q^2\left[\frac{N_c}{\tau_c} + (\langle\tilde{E}_{cv}\rangle + \langle\tilde{E}_{vc}\rangle)\langle\hat{n}\rangle\right]$$
$$\sim 2qI + 4q^2\langle\tilde{E}_{vc}\rangle\langle\hat{n}\rangle. \tag{5.9}$$

This current-noise source is higher than the usual shot-noise level. The excess noise, i.e., the second term of expression (5.9), stems from the fact that the average junction current is given by the difference between the stimulated emission and the absorption rate, but the current noise is contributed by these two processes independently.[46,47] Note that this current-noise source represents fluctuations that are due to spontaneous emission, stimulated emission, and absorption, yet it does not include the so-called pump fluctuation. Expression (5.9) is sometimes erroneously interpreted as the pump fluctuation in a semiconductor laser, corresponding to the shot noise of the pump light in a conventional laser. If we compare expression (5.9) with Eq. (4.5), the pump fluctuation term $\langle\tilde{P}\rangle$ is apparently absent in expression (5.9). The shot-noise current in a p–n junction[48,49] is not the noise associated with the pump source (such as chemical process of a battery) but is the consequence of the fluctuation events inside the diode.

Let R_s denote the sum of the source resistance and the diode's series resistance. Then the associated voltage-noise source V_s with R_s represents the thermal fluctuation of majority carrier flow. Its low-frequency spectrum is given by

$$S_{V_s}(\Omega) \sim 4k_BTR_s. \tag{5.10}$$

i_n and v_n represent the junction-current fluctuation and junction-voltage fluctuation. i_L is the so-called photon-current fluctuation defined by[47]

$$i_L = q(\langle\tilde{E}_{cv}\rangle - \langle\tilde{E}_{vc}\rangle)2\langle A\rangle\Delta A. \tag{5.11}$$

L and R_{se} represent the coupling between the cavity internal photon fluctuation and the population-difference fluctuation and are expressed as

$$L = \frac{mV_T\tau_{st}}{qN_c(\langle\tilde{E}_{cv}\rangle - \langle\tilde{E}_{vc}\rangle)} \tag{5.12}$$

and

$$R_{se} = L[\gamma - (\langle\tilde{E}_{cv}\rangle - \langle\tilde{E}_{vc}\rangle)]. \tag{5.13}$$

The voltage-noise source v represents the noise driving sources for the photon field. The low-frequency spectrum of v is given by

$$S_v(\Omega) = 2q^2(\langle\tilde{E}_{cv}\rangle - \langle\tilde{E}_{vc}\rangle)^2L^2[(\langle\tilde{E}_{cv}\rangle + \langle\tilde{E}_{vc}\rangle)\langle\hat{n}\rangle + \gamma\langle\hat{n}\rangle]. \tag{5.14}$$

The two noise sources i and v are partly correlated,

$$S_{iv}(\Omega) \equiv \langle i(\Omega)v(\Omega)\rangle = -2q^2(\langle\tilde{E}_{cv}\rangle^2 - \langle E_{vc}\rangle^2)L\langle\hat{n}\rangle. \tag{5.15}$$

The circuit equation (5.11) for i_L and that for $v_n = (q/C)\Delta\tilde{N}_c$ are rewritten as the equations of motion for the cavity-internal-field amplitude fluctuation $\Delta\hat{A}$ and the population-difference fluctuation $\Delta\tilde{N}_c$:

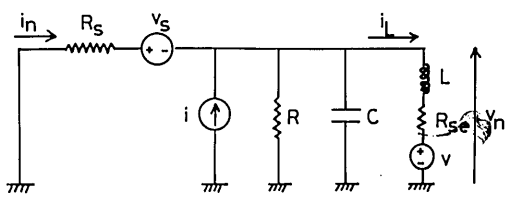

Fig. 13. Noise-equivalent circuit of a semiconductor-laser diode.

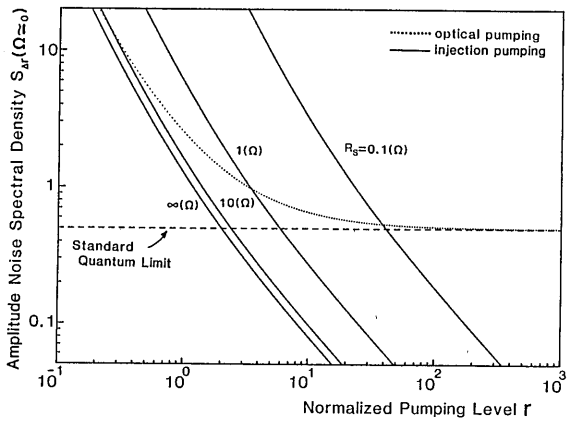

Fig. 14. Amplitude noise spectra as a function of normalized pump level r and source resistance, R_s.

$$\frac{d}{dt} i_L = \frac{v_n - v}{L} - \frac{R_{se}}{L} i_L$$

$$\rightarrow \frac{d}{dt} \Delta\hat{A} = -[\gamma - (\langle \tilde{E}_{cv} \rangle - \langle \tilde{E}_{vc} \rangle)]\Delta\hat{A} + \frac{1}{2\langle A \rangle \tau_{st}} \Delta\tilde{N} + (\hat{G}_r + \sqrt{\gamma_e} \hat{f}_r) \tag{5.16}$$

and

$$\frac{d}{dt} v_n = -\frac{1}{C}\left(\frac{1}{R} + \frac{1}{R_s}\right) v_n - \frac{i_L}{C} + \frac{i}{C} - \frac{v}{CR_s},$$

$$\frac{d}{dt} \Delta\tilde{N}_c = -\left(\frac{1}{\tau_{sp}} + \frac{1}{\tau_{CR}}\right) \Delta\tilde{N}_c - (\langle \tilde{E}_{cv} \rangle - \langle \tilde{E}_{vc} \rangle) 2\langle \hat{A} \rangle \Delta\hat{A} + \tilde{F}_c' + \tilde{F}_{th}. \tag{5.17}$$

Here the low-frequency spectra for $\tilde{F}_c'$ and $\tilde{F}_{th}$ are given by

$$S_{\tilde{F}_c'}(\Omega) = 2\left[\frac{\langle \hat{N}c \rangle}{\tau_{sp}} + (\langle \tilde{E}_{cv} \rangle + \langle \tilde{E}_{vc} \rangle)\langle \hat{n} \rangle\right] \tag{5.18}$$

and

$$S_{\tilde{F}_{th}}(\Omega) = \frac{4V_T}{qR_s}. \tag{5.19}$$

Equations (5.16) and (5.17) are similar to conventional equations, but they differ in the following two respects:

(1) There is an additional decay rate, $1/\tau_{CR} = 1/CR_s$, for the population-difference fluctuation.

2. The shot-noise-limited pump-amplitude fluctuation term is replaced by the thermal noise of R_S.

When R_S is very small, the population difference is pinned by the new decay process. This corresponds to the constant voltage operation of the diode. By contrast, when R_S is very large, the pump-fluctuation term is suppressed. This corresponds to the constant current operation of the diode. The criterion for reducing pump fluctuations below the shot-noise limit is given by

$$S_{F_{th}}(\Omega) = \frac{4V_T}{qR_s} < 2qI \rightarrow R_S > 2R. \tag{5.20}$$

Since the diode's differential resistance monotonically decreases with increasing pump level, Eq. (5.20) will eventually be satisfied with increasing pumping for any small R_S value.

The output-field-amplitude spectral density in the low-frequency region versus the pump rate is plotted in Fig. 14 as a function of the R_S value. The amplitude spectral density for a conventional laser with shot-noise-limited pump fluctuation is also plotted for comparison.

C. Observation of Amplitude Squeezing in a Semiconductor Laser

An InGaAsP/InP distributed-feedback semiconductor laser (DFB-SL) with a 1.56-μm oscillation wavelength was measured by the setup shown in Fig. 15. The DFB-SL featured stable single-longitudinal-mode operation, and side-mode intensity was suppressed by more than 30 dB (to less than 0.1%). The laser had a buried heterostructure and a short cavity (80–110 μm) to produce a low-threshold current. It also had an antireflection coating on the front facet and a high-reflection coating on the rear facet to achieve high quantum efficiency. The laser must have a low-threshold current for saturation-free operation of the photodetectors, even at a high pump rate, and a high quantum efficiency to feature large-amplitude squeezing.

An InGaAs/InP photodiode with 300-μm diameter and 550-MHz bandwidth was used as a detector. The detector surface is slanted from the optical path to avoid optical reflection feedback to the laser. An optical isolator with 30-dB isolation was inserted between the laser and the detector, because even a minute amount of scattered light fed back from the detector surface to the laser can cause excess amplitude noise. The detector quantum efficiency η_c, including insertion losses for a collimated lens and isolator, is about 22%.

The SQL was calibrated by a balanced receiver.[50] The test laser output was blocked, and a polarization beam splitter was inserted in front of two identical InGaAs/InP photodiodes. A high-power (>20-mW) InGaAsP/InP DFB-SL (reference laser) output was attenuated by more than 10 dB and illuminated onto the two photodiodes to produce exactly the same photocurrents as did the test laser. Precise adjustment of the two detector currents was realized by a half-wavelength plate and a polarization beam splitter. The excess amplitude noise of the reference laser beam was smaller by −1 dB than the SQL at the photodiode front end. A balanced receiver's excess-noise-suppression factor is

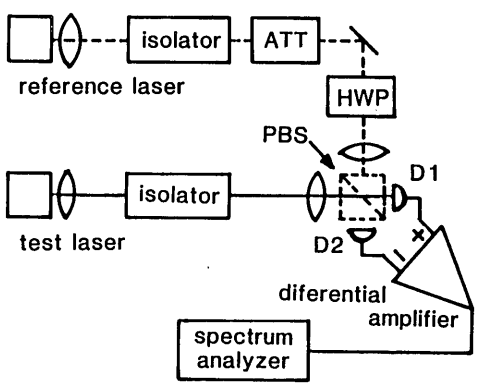

Fig. 15. Experimental setup for measuring the amplitude noise spectrum. HWP, half-wavelength plate; PBS, polarization beam splitter; ATT, optical attenuator; D1, D2, detectors.

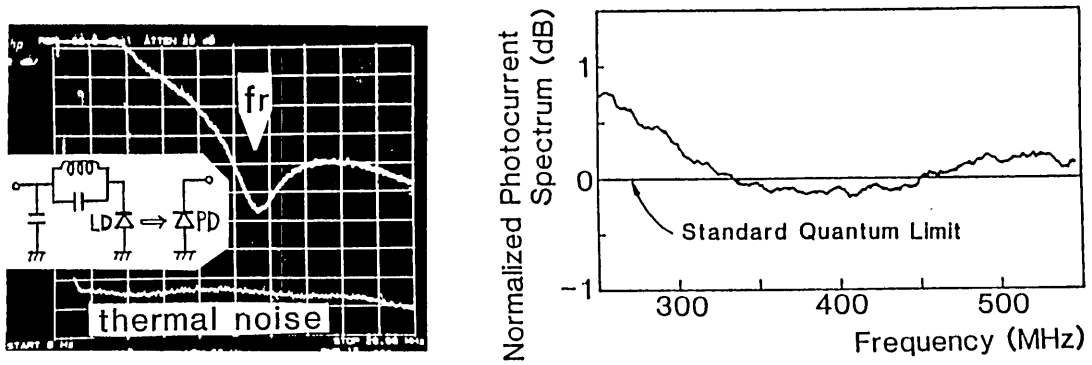

Fig. 16. (a) Photocurrent spectrum for the bias-circuit-driven laser shown in the inset. A high source impedance is realized only at the LC-circuit resonant frequency f_r. (b) Photocurrent spectrum normalized by SQL at a pump level of 3.9 times threshold. The bias circuit features a high source impedance (750 Ω) near 400 MH_z. LD, laser diode; PD, photodiode.

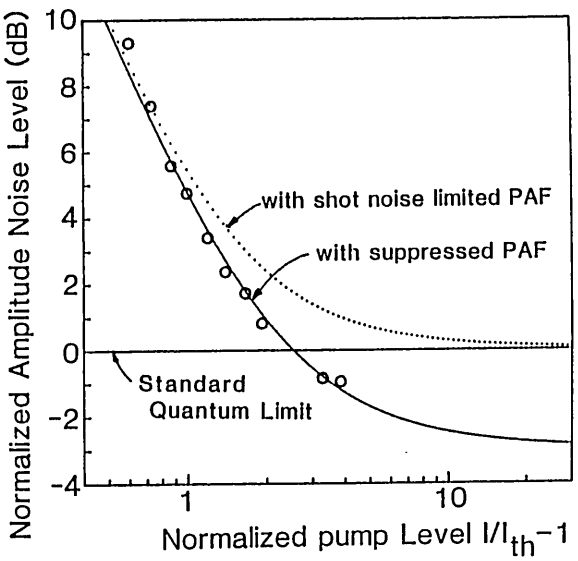

Fig. 17. Theoretical (solid line) and experimental (open circles) amplitude noise levels versus pump level for $R_s = 750\ \Omega$. The dotted line is the theoretical amplitude noise level for a laser with a shot-noise-limited pump fluctuation.

greater than 18 dB in the frequency range from dc to 550 MHz. Accordingly, the excess amplitude noise in the reference laser was suppressed below the SQL by more than 19 dB, so that the error in this calibration of the SQL is less than 0.05 dB (1.3%).[22]

The experimental result shown in Fig. 16(a) demonstrates the photocurrent noise suppression by this principle. The bias circuit features a high source impedance only at the LC-circuit resonant frequency f_r. (The photocurrent spectrum is actually reduced at f_r.) On the contrary, when the bias circuit is replaced by the LC circuit that features a low source impedance at the LC-circuit resonant frequency f_r, the photocurrent spectrum is reduced, except at f_r.

The photocurrent spectrum for $r \equiv I/I_{th} - 1 = 3.9$ is compared with the SQL in Fig. 16(b). The bias circuit in this measurement has a source impedance of 750 Ω over a broad frequency range centered at 400 MHz. This frequency region is well above the cutoff of $1/f$ noise and residual mode-competition noise. It is also well below the relaxation-oscillation resonance. The photocurrent spectrum between 350 and 450 MHz is reduced to below the SQL. The maximum noise reduction occurs at a frequency near 400 MHz and is 0.33 dB (7.3%) in power below the SQL, and the average noise reduction in the frequency range between 350 and 450 MHz is 0.18 dB (4.1%). The results correspond to 1.6-dB (31%) maximum noise reduction and 1.0-dB (21%) average noise reduction at the laser output if the effect of detector quantum efficiency η_c is compensated for.

The average amplitude noise, corrected for detector quantum efficiency versus pump level r, is in good agreement with the theoretical predictions, as shown in Fig. 17. The theoretical amplitude noise for a laser with shot-noise-limited pump fluctuation is also plotted for comparison. It is clear from this result that a constant-current-driven semiconductor laser is different from an ordinary optical pumped laser.

The laser used in this experiment has a relatively small differential quantum efficiency ($\eta_D \sim 0.3$) that is due to nonradiative (Auger) carrier recombination and free-carrier photon-absorption processes. This limits the amplitude squeezing obtained when $r \gg 1$. These two loss effects can be suppressed by cooling the laser or by increasing its output coupling loss.

6. CONCLUSION

Four different NUS generation schemes were discussed. They are the following: (1) unitary evolution using self-phase modulation and interference, (2) nonunitary state reduction by QND photon-number measurement or parametrically amplified idler photon counting, (3) negative-feedback oscillators, and (4) pump-noise-suppressed lasers. A near NUS has actually been generated by the fourth scheme, i.e., by an InGaAsP/InP DFB laser driven by a constant-current source. The observed noise level corrected for the detector quantum efficiency is 1 dB (20%) below the SQL in a wide frequency range between 350 and 450 MHz. A semiconductor laser has a potential capability to produce a broadband NUS from dc to several gigahertz if it is properly designed. The low-temperature operation of a microcavity and quantum-well-structure semiconductor laser has already confirmed this.[51]

The generation of a NUS in a pump-noise-suppressed laser oscillator is similar in principle to the generation of sub-Poissonian light in a micromaser consisting of a superconducting high-Q cavity and a Rydberg atom.[52,53] It also resembles the Bloch and Josephson oscillations in a microsuperconducting junctions.[54] The clarification of these relations may shed light on the fundamental quantum-mechanical issues (microscopic to macroscopic transition or quan-

tum-mechanical to classical transition), but these remain to be explored in the future.

ACKNOWLEDGMENTS

The authors wish to thank H. A. Haus of the Massachusetts Institute of Technology, O. Nilsson of the Royal Institute of Technology, Stockholm, and H. P. Yuen of the Northwestern University for their continued interest in this work and useful discussions.

* On leave from the Royal Institute of Technology, Stockholm, Sweden.

REFERENCES

1. D. Bohm, *Quantum Theory* (Prentice-Hall, Englewood Cliffs, N.J., 1951).
2. A. Messiah, *Quantum Mechanics* (McGraw-Hill, New York, 1961).
3. H. Takahashi, Adv. Commun. Syst. **1,** 227 (1965).
4. D. Stoler, Phys. Rev. D **4,** 1925 (1971).
5. H. P. Yuen, Phys. Rev. A **13,** 2226 (1976).
6. D. F. Walls, Nature **306,** 141 (1983).
7. R. J. Glauber, Phys. Rev. **131,** 2766 (1963).
8. R. J. Glauber, *Quantum Optics and Electronics*, C. DeWitt, A. Blandin, and C. Cohen-Tannoudji, eds. (Gordon & Breach, New York, 1965), p. 65.
9. R. Jackiw, J. Math. Phys. **9,** 339 (1968).
10. P. Carruthers and M. M. Nieto, Rev. Mod. Phys. **40,** 411 (1968).
11. Y. Yamamoto and H. A. Haus, Rev. Mod. Phys. **56,** 1001 (1986).
12. K. Igeta and Y. Yamamoto, "Quantum mechanical optical computers," tech. paper on optics and quantum electronics (Institute of Electronics and Communication Engineers of Japan, Tokyo, 1987.
13. H. P. Yuen, Phys. Rev. Lett. **56,** 2176 (1986).
14. R. E. Slusher, L. W. Hollberg, B. Yurke, J. C. Mertz, and J. F. Valley, Phys. Rev. Lett. **55,** 2409 (1985).
15. R. M. Shelby, M. D. Levenson, S. H. Perlmutter, R. G. DeVoe, and D. F. Walls, Phys. Rev. Lett. **57,** 691 (1986).
16. L. A. Wu, H. J. Kimble, J. L. Hall, and H. Wu, Phys. Rev. Lett. **57,** 2520 (1986).
17. M. W. Maeda, P. Kumar, and J. H. Shapiro, Opt. Lett. **12,** 161 (1987).
18. M. Kitagawa and Y. Yamamoto, Phys. Rev. A **34,** 3974 (1986).
19. M. Kitagawa, N. Imoto, and Y. Yamamoto, Phys. Rev. A **35,** 5270 (1987).
20. N. Imoto, H. A. Haus, and Y. Yamamoto, Phys. Rev. A **32,** 2287 (1985).
21. C. K. Hong and L. Mandel, Phys. Rev. Lett. **56,** 58 (1986).
22. S. Machida and Y. Yamamoto, Opt. Commun. **57,** 290 (1986); Y. Yamamoto, N. Imoto, and S. Machida, Phys. Rev. A **33,** 3243 (1986); H. A. Haus and Y. Yamamoto, Phys. Rev. A **34,** 270 (1986).
23. J. G. Walker and E. Jakeman, Proc. Soc. Photo-Opt. Instrum. Eng. **492,** 274 (1985); E. Jakeman and J. G. Rarity, Opt. Commun. **59,** 219 (1986); J. G. Walker and E. Jakeman, Opt. Acta **32,** 1303 (1985).
24. B. E. A. Saleh and M. C. Teich, Opt. Commun. **52,** 429 (1985).
25. Y. Yamamoto, S. Machida, and O. Nilsson, Phys. Rev. A **34,** 4025 (1986).
26. Y. Yamamoto and S. Machida, Phys. Rev. A **35,** 5114 (1987).
27. S. Machida, Y. Yamamoto, and Y. Itaya, Phys. Rev. Lett. **58,** 1000 (1987).
28. H. P. Yuen and J. H. Shapiro, Opt. Lett. **4,** 334 (1979).
29. B. L. Schumaker, Phys. Rep. **135,** 318 (1986).
30. W. Pauli, *Handbuch der Physik* (Springer-Verlag, Berlin, 1958), Vol. V.
31. J. von Neumann, *Mathematical Foundations of Quantum Mechanics* (Princeton U. Press, Princeton, N.J., 1955).
32. V. B. Braginsky, Y. I. Vorontsov, and K. S. Thorne, Science **209,** 547 (1980).
33. C. M. Caves, K. S. Thorne, R. W. P. Drever, V. D. Sandberg, and M. Zimmerman, Rev. Mod Phys. **52,** 341 (1980).
34. G. J. Milburn and D. F. Walls, Phys. Rev. A **28,** 2015 (1983).
35. J. H. Shapiro, M. C. Teich, B. E. A. Saleh, P. Kumar, and G. Saplakogln, Phys. Rev. Lett. **56,** 1136 (1986).
36. J. H. Shapiro, G. Saplakoglu, S.-T. Ho, P. Kumar, B. E. A. Saleh, and M. C. Teich, "Theory of light detection in the presence of feedback," J. Opt. Soc. Am. B **4,** 1604 (1987).
37. H. Haken, *Encyclopedia of Physics* (Springer-Verlag, Berlin, 1970), Vol. 25/2c.
38. M. Sargent III, M. O. Scully, and W. E. Lamb, Jr, *Laser Physics* (Addison-Wesley, Reading, Mass., 1974).
39. C. W. Gardiner and M. J. Collet, Phys. Rev. A **31,** 3761 (1985).
40. Y. Yamamoto and N. Imoto, IEEE J. Quantum Electron. **QE-22,** 2032 (1986); O. Nilsson, Y. Yamamoto, and S. Machida, IEEE J. Quantum Electron. **QE-22,** 2043 (1986).
41. N. Imoto and Y. Yamamoto, in *Digest of Conference on Lasers and Electro-Optics* (Optical Society of America, Washington, D.C., 1986), paper ThE4; N. Imoto, S. Watkins, and Y. Sasaki, Opt. Commun. **61,** 159 (1987).
42. M. D. Levenson, R. M. Shelby, M. Reid, and D. F. Walls, Phys. Rev. Lett. **57,** 2473 (1986).
43. G. Björk and Y. Yamamoto, "Generation and amplification of number states by nondegenerate parametric oscillators with idler measurement feedback," Phys. Rev. A (to be published).
44. M. Teich and B. E. A. Saleh, J. Opt. Soc. Am. B **2,** 275 (1985).
45. S. M. Sze, *Physics of Semiconductor Devices* (Wiley, New York, 1969).
46. H. Huang, Z. Phys. **206,** 163 (1967).
47. C. Harder, J. Katz, S. Margalit, J. Shacharr, and A. Yariv, IEEE J. Quantum Electron. **QE-18,** 333 (1982).
48. A. van der Ziel, *Fluctuation Phenomena in Semiconductors* (Butterworth, London, 1959).
49. M. J. Buckingham, *Noise in Electronic Devices and Systems* (Wiley, New York, 1983).
50. H. P. Yuen and V. W. S. Chan, Opt. Lett. **8,** 177 (1983); G. L. Abbas, V. W. S. Chan, and T. K. Yee, Opt. Lett. **8,** 419 (1983); S. Machida and T. Yamamoto, IEEE J. Quantum Electron. **QE-22,** 617 (1986).
51. S. Machida and Y. Yamamoto, "Amplitude squeezing in semiconductor lasers," tech. paper on optics and quantum electronics (Institute of Electronics and Communication Engineers of Japan, Tokyo, 1987).
52. J. Krause, M. O. Scully, and H. Walther, Phys. Rev. A **34,** 2032 (1986).
53. P. Filipowicz, J. Javanainen, and P. Meystre, Phys. Rev. A **34,** 3077 (1986).
54. D. V. Avelin and K. K. Likharev, J. Low Temp. Phys. **62,** 345 (1986).

Y. Yamamoto

Y. Yamamoto was born in Tokyo, Japan, on November 21, 1950. He received the B.S. degree from the Tokyo Institute of Technology, Tokyo, in 1973 and the S.M. and Ph.D. degrees from the University of Tokyo in 1975 and 1978, respectively. Since joining the NTT Electrical Communication Laboratories, Musashino, Tokyo, in 1978, he has been engaged in research on coherent communication, optical amplifiers, squeezed states, and QND measurement. He is now a Yamamoto Research Group Leader with the NTT Basic Research Laboratory. He is the author or coauthor of about 60 technical papers and 5 books. He was a visiting scientist at the Research Laboratory of Electronics, Massachusetts Institute of Technology, Cambridge, between 1982 and 1983. Dr. Yamamoto is a member of the Institute of Electronics and Communication Engineers of Japan, the Japan Society of Applied Physics, the Physical Society of Japan, and the Institute of Electrical and Electronics Engineers.

S. Machida

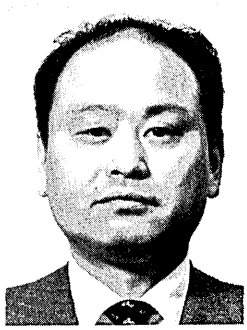

S. Machida was born in Tokyo, Japan, on August 3, 1942. He received the B.S. degree from Tokyo Electrical Engineering College, Tokyo, in 1967. He joined Electrical Communication Laboratories, Nippon Telegraph and Telephone Public Corporation in 1961, and has engaged in research and development of traveling-wave tubes, microwave integrated circuits, components for millimeter-wave transmission systems, and pulse-circuit elements using the Gunn effect and optical transmission systems. Currently he is working on SS's and QND measurement at NTT Musashino Electrical Communication Laboratories, Musashino, Tokyo, where he is a research engineer at the Basic Research Laboratory. Mr. Machida received the Fourteenth Prize of the Minister of Science and Technology in 1973 for his work on improvement of components for millimeter-wave transmission systems.

N. Imoto

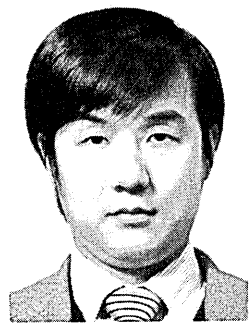

N. Imoto was born in Kumamoto, Japan, on October 17, 1952. He received the B.S. and M.S. degrees in applied physics from the University of Tokyo in 1975 and 1977, respectively. Since joining the NTT Electrical Communication Laboratories, Musashino, Tokyo, in 1977, he has been engaged in research on optical-fiber communications, quantum optics, cooperative phenomena, and QND measurement. Mr. Imoto is a member of the Physical Society of Japan, the Japan Society of Applied Physics, and the Institute of Electronics and Communication Engineers of Japan.

Masahiro Kitagawa

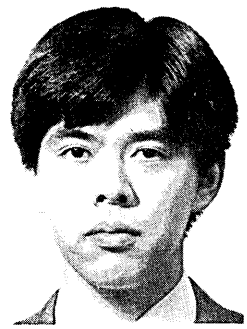

M. Kitagawa was born in Osaka, Japan, on September 28, 1958. He received the B.S. and M.S. degrees in electronic engineering from Osaka University, Osaka, in 1981 and 1983, respectively. Since joining NTT Basic Research Laboratories, Nippon Telegraph and Telephone Corporation, Tokyo, in 1983, he has been engaged in research on artificial birefingence, ultrashort-light-pulse generation, and quantum and nonlinear optics. Mr. Kitagawa is a member of the Physical Society of Japan and the Japan Society of Applied Physics.

G. Björk

Gunnar Björk was born in Gothenburg, Sweden, on November 25, 1958. He received the M.S. degree in engineering physics in 1984 from the Royal Institute of Technology, Stockholm, Sweden. He is currently pursuing the Ph.D. degree in fiber optics. His research interests are in semiconductor-laser properties, coherent optical systems, and quantum optics. Currently he is visiting Dr. Yamamoto's group at NTT.